Response Functions in the Theory of Raman Scattering by Vibrational and Polariton Modes in Dielectric Crystals

A. S. BARKER, JR., R. LOUDON*
Bell Telephone Laboratories, Incorporated, Murray Hill, New Jersey 07971

The paper begins with a tutorial introduction to the theory of inelastic light scattering by polaritons in dielectric crystals. The treatment is based on a simple two-oscillator model which represents the ionic and electronic motions of a crystal. The model contains a third-order anharmonicity which allows an incident laser beam to mix with the oscillator fluctuations and produce scattered light of frequency different from the incident frequency. The magnitude of the oscillator fluctuations is determined by an application of the Nyquist or fluctuation-dissipation theorem, using the response functions of the oscillators for externally applied forces. The simple model gives results for light scattering cross sections which agree with more rigorous derivations in the existing literature. The response function approach is generalized to apply to crystals having many ionic resonances and of uniaxial or orthorhombic structure. The general formulas reduce in appropriate special cases to results already published. Experimental and theoretical work on light scattering by polaritons and by pure phonons is reviewed in the context of both the two-oscillator model and the general theory. Particular attention is given to resonance scattering in an attempt to achieve consistency between the differing theoretical treatments in the literature. The subject matter of the review overlaps some topics in nonlinear optics, and contact is made with the theories of the electrooptic effect and stimulated Raman scattering.

CONTENTS

1. RESPONSE FUNCTIONS AND FLUCTUATIONS

A. Introduction

It has been recognized since the pioneering work of Huang (1951) and Poulet (1955) that lattice vibrations which carry an electric dipole moment have radically different properties from nonpolar vibrations. The dipole moment couples the lattice vibration to the radiation field in the crystal to form mixed excitation modes, part phonon and part photon, which have a characteristic dispersion relation and are known as polaritons. The excitations can be explored in their most interesting long-wavelength region by inelastic light scattering experiments. They have frequencies which depend in general on their wave-vector magnitude, and direction relative to the crystal axes and on their polarization. Their observed degeneracies are usually smaller than group theory would predict, and the relative intensity of scattering by the split components of a group theoretically degenerate excitation is not correctly predicted by a theory based on the crystal symmetry group. In contrast, the light scattering by nonpolar vibrations shows that the excitations have frequencies independent of wave vector, and the degeneracies and polarization dependence of the scattered intensity are in good agreement with the predictions of group theory.

The development of the theory of light scattering by polar vibrations in the years since Poulet first identified the source of their apparently anomalous properties has been somewhat piecemeal. Various papers have inched forward the general theory by treating a range of special cases, covering one by one the different symmetries of crystals, and concentrating on some particular aspects of the scattering.

We have three main intentions in the present paper: first, to present a tutorial introduction to the theory of light scattering by polaritons using what seems to us to be the simplest model of a crystal which is capable of producing realistic results; second, to present a theory of the scattering sufficiently general to embrace all the previous work in the area and to apply to any crystal whose principal axes are at right angles; and finally to show how the fluctuations in the crystal which

* Permanent address: Physics Department, Essex University, Colchester, England.

give rise to the scattering can be obtained very easily using the fluctuation-dissipation theorem.

Since all the calculations are based on this theorem, we complete Sec. 1 by reviewing briefly the Nyquist or fluctuation-dissipation theorem, which relates the mean-square fluctuation in some physical quantity to the imaginary part of an appropriately defined admittance or response function.

In Sec. 2 we introduce a simple model of a crystal in which the lattice and electronic motions are each represented by a simple harmonic oscillator. The admittances required for the Raman crossection are easily obtained by calculating the response of the model to external forces applied to the ionic and electronic oscillators. The polariton frequencies, determined by the poles of the admittances, are discussed. The model is now made nonlinear by adding to it an anharmonic potential which couples the two oscillators. The anharmonicity is assumed sufficiently weak that its effects can be treated by first-order perturbation theory. With anharmonicity included, the two-oscillator model can couple light waves of different frequency, and displays the various properties studied in nonlinear optics. The model is in fact similar to, but somewhat simpler than, one used by Garrett (1968) in a discussion of nonlinear susceptibilities for various optical processes. Our main concern is with light scattering rather than with nonlinear optics as such, but as a first application of the anharmonic model we derive an expression for the electrooptic coefficient and make contact with the literature of nonlinear optics. Finally, in Sec. 2 we derive the intensity of light scattering by the model crystal. The scattering of an incident laser beam arises from its mixing with the crystal fluctuations to produce light of various shifted frequencies. The scattering cross section is related to the mean-square fluctuations in oscillator amplitude, and can then be evaluated using the response functions derived earlier in the section. The polariton light-scattering cross section so derived displays all the features found in more complicated derivations. The simple model calculation enables a clearer understanding of the origins of the various terms in the cross section.

In Sec. 3, we leave the two-oscillator model and consider the more general case of a crystal having an arbitrary number of polar lattice vibration modes and possessing orthorhombic symmetry. The treatment parallels that of Sec. 2 to a large extent. Response functions are derived for the more complicated crystal by considering externally applied polarization and externally applied forces. The polariton dispersion relations are derived by finding the poles of the response function and reducing them to results given by previous authors when specialized to uniaxial or cubic crystal symmetry. The electrooptic coefficient and scattering cross section are derived using the response functions and the fluctuation-dissipation theorem.

The theories of Secs. 2 and 3 are applied in Sec. 4 to reviews of experimental and theoretical work on light scattering by polaritons and vibrational modes. For the usual right-angle scattering geometry the cross-section formulas simplify and can be compared with experiment. Scattering experiments at small angles are required to observe the more interesting regions of the polariton dispersion curves; such experiments are more difficult to carry out and not all aspects of the theory have so far been subjected to experimental test. We review the existing experimental work and derive sum rules and linewidth expressions for the polaritons which can in principle be tested experimentally. We also emphasize the properties of polaritons in biaxial orthorhombic crystals. The resonance Raman effect, where the laser frequency lies close to an electronic transition frequency of the crystal, is a field of much current interest. A number of theoretical papers have considered the case of resonance with an isolated exciton transition, and several conflicting or apparently conflicting expressions have been derived. We treat the same problem within the context of the theory of the present paper and achieve a reconciliation between the previous workers in the field. Finally we consider briefly the related process of stimulated Raman scattering, and derive an expression for the stimulated gain in scattering by polaritons. The result agrees with expressions previously derived by the methods of nonlinear optics.

B. Nyquist's Theorem for Raman Scattering

The frequency spectrum of fluctuations in a variable W is given by the quantum mechanical Nyquist formula

$$\langle |W|^2\rangle_\omega = (\hbar/\pi)[n(\omega)+1]\,\mathrm{Im}\,(\mathbf{T}), \qquad (1.1)$$

where Im $(\mathbf{T})$ is the imaginary part of the linear response function $\mathbf{T}$ appropriate to the variable W, and $n(\omega)$ is the quantum mechanical thermal factor

$$n(\omega) = [\exp(\hbar\omega/k_BT)-1]^{-1}. \qquad (1.2)$$

Here k_B is the Boltzman constant, and T is the absolute temperature.[1,2] The frequency domain ranges from minus infinity to infinity in both above equations so that the mean square value of the fluctuating variable W is given by

$$\langle W^2(t)\rangle_{Av} = \int_{-\infty}^{\infty} \langle |W|^2\rangle_\omega \, d\omega. \qquad (1.3)$$

[1] An excellent elementary review of fluctuation theory and power spectra has been given by D. K. C. MacDonald (1962).

[2] Most derivations of the fluctuation spectrum (1.1) obtain the thermal factor $n(\omega)+\frac{1}{2}=(\frac{1}{2})\coth(\omega/2)$ rather than $n(\omega)+1$. This is because a symmetric combination of $+\omega$ and $-\omega$ Fourier components is averaged and all integrals are then folded and taken to range from zero to infinity. In Raman scattering, $+\omega$ and $-\omega$ can be measured separately so that one sided integrals are not appropriate. Butcher and Ogg (1965) first pointed out the correct thermal factor in Nyquist's theorem as applied to Raman scattering. The thermal factor in (1.1) removes the zero-point fluctuation noise which cannot be detected by the usual radiation detector which only annihilates photons.

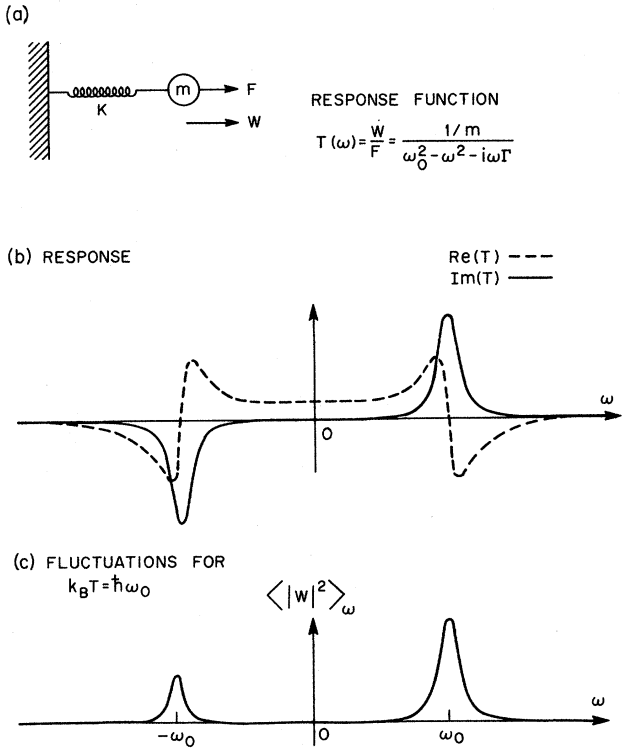

FIG. 1. (a) Mechanical oscillator driven by force F and having its resonance at $\omega_0=(K/m)^{1/2}$. The response function has damping (Γ) included to broaden the resonance. (b) Real and imaginary parts of the response function. (c) Fluctuation spectrum of the displacement W for the temperature indicated.

In words, Nyquist's theorem states that the power spectrum of the fluctuations[1] in $W(t)$ is related to the product of a thermal factor and the resistive (dissipative) part of the corresponding response function, Im ($\mathbf{T}$). Derivations of (1.1) have been given by Landau and Lifshitz (1969),[2] and Benson and Mills (1970a).

Figure 1 shows the response function and fluctuation spectrum for a simple harmonic oscillator. The displacement is W, the restoring force constant K, and the mass m. The damping constant Γ is included to give the response finite linewidth. The mechanical response function $\mathbf{T}$[3] is simply the displacement per unit force and has the familiar resonance form given in the figure. $\mathbf{T}$ has real and imaginary parts which are symmetric and antisymmetric respectively.[4] If for convenience we choose a temperature T such that $\hbar\omega_0=k_BT$, the fluctuation spectrum (1.1) appears as shown in Fig. 1(c).

It will be shown in Sec. 2 that for a simple model of Raman scattering by phonons, Fig. 1(c) shows essentially the scattered light spectrum which is measured. Figure 2(a) is a schematic diagram of a Raman scattering experiment. A laser with frequency ω_l is used as the source or pump. The laser beam is directed through the sample which is transparent at the laser frequency. Ninety degree scattered light is picked up by a lens and analyzed by a spectrometer. If the sample has a Raman-active phonon mode described by the oscillator of Fig. 1, then the scattered spectrum is centered at ω_l with a strong Stokes peak at $\omega_l-\omega_0$ and a weaker anti-Stokes peak at $\omega_l+\omega_0$. The Stokes peak corresponds to down-scattering where a phonon is created. Phonon creation is described by $+\omega_0$, but causes a frequency shift of $-\omega_0$ in the Raman spectrum since the scattered photon must have energy $\hbar\omega_l-\hbar\omega_0$ to conserve energy. The anti-Stokes peak corresponds to phonon destruction and approaches zero strength as the temperature approaches zero. Note that when ω changes sign

$$n(-\omega)+1=-n(\omega) \qquad (1.4)$$

so that the thermal factor in 1.1 correctly reproduces the usual Stokes ($n+1$) and anti-Stokes (n) thermal factors. Comparison of Figs. 1 and 2 immediately shows the importance of the fluctuation spectrum of the phonon coordinate W in understanding Raman spectra, since the lower graphs in each figure are essentially identical.

Note that two important ingredients are necessary to establish the fluctuation spectrum and hence the Raman scattering spectrum. First there is the linear response function $\mathbf{T}$ which contains details of mode frequency and linewidth. For a simple harmonic oscillator $\mathbf{T}$ can be calculated classically. Second, the

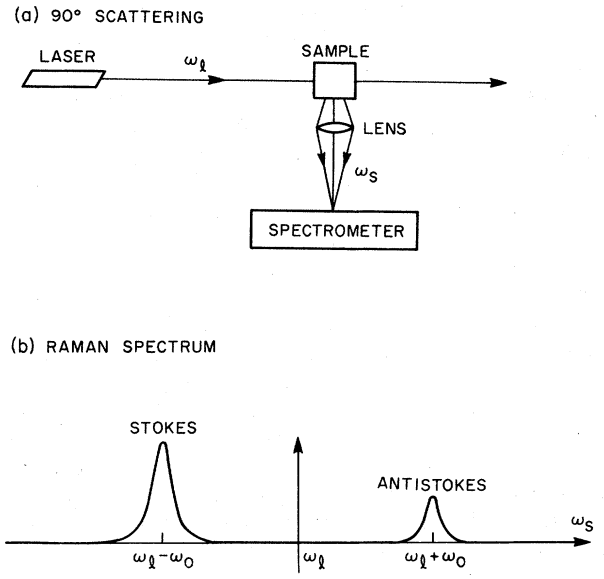

FIG. 2. (a) Schematic diagram of 90 degree Raman scattering. (b) Raman scattered spectrum for a sample possessing one Raman active phonon mode described by the oscillator of Fig. 1 at temperature $k_BT=\hbar\omega_0$.

[3] We write $\mathbf{T}$ as a matrix for consistency with later usage though for the one-dimensional oscillator of Fig. 1, $\mathbf{T}$ has dimension one by one.

[4] More generally, $\mathbf{T}(-\omega^*)=\mathbf{T}^*(\omega)$, where * denotes complex conjugate (Landau and Lifshitz 1969).

quantum-thermal factor is needed to describe the proper weighting of processes where an excitation is created or destroyed.

In the high-temperature (i.e., classical) limit, Nyquist's theorem takes the simple form

$$\langle |W|^2\rangle_\omega = (k_BT/\pi\omega)\ \mathrm{Im}\ (\mathbf{T}). \quad \text{high temperature limit.} \tag{1.5}$$

A familiar statement of (1.5) is the equation for voltage fluctuations across a two terminal impedance

$$\langle |V|^2\rangle_\omega = (k_BT/\pi)\ \mathrm{Re}\ (\mathbf{Z}), \tag{1.6}$$

where Z is the electrical impedance. Equation (1.6) differs in form from (1.5) only because electrical response functions (e.g., impedance) differ by a time derivative[5] from the response functions employed in most other systems. Equation (1.6) is historically important as the original Nyquist theorem developed to explain voltage fluctuations (Johnson noise) in electrical networks. Table I shows the variables usually used in mechanical and electrical systems, and collects various forms of Nyquist's theorem. It also lists our conventions for Fourier components and complex time factors. Throughout this paper we will refer to $\mathbf{T}$ somewhat loosely as a response function or as an admittance.

For a system with several independent variables W_1, W_2, etc., correlations between variables must be considered. Landau and Lifshitz (1969) and Lax (1960) have shown that the Nyquist theorem has the form

$$\langle W_i^* W_j\rangle_\omega = \langle W_i W_j^*\rangle_\omega = (k_BT/\pi\omega)\ \mathrm{Im}\ [T_{ij}(\omega)] \tag{1.7}$$

in the classical limit. In the one-variable case when $i=j$, Equation (1.5) is recovered for the fluctuations. The new terms are the cross correlations which exist only if there is coupling between variables, described by the response function T_{ij}.[6] In one model of Raman scattering discussed in Sec. 2, $\langle W_1^* W_2\rangle$ describes the correlation between the ion and electron motion; $T_{12}(\omega)$ is then the response of the electron to an external force on the ion. The existence of a finite T_{12}, (i.e., of correlations between W_1 and W_2) can give interesting cancellations in the Raman spectrum.

The main purpose of the present work is to examine the various linear response functions or admittances T_{ij} appropriate to Raman scattering. The models to be examined assume that the nonlinearities which cause Raman scattering are small so that the linear response is not affected. An alternative approach is to calculate the fluctuations from the imaginary part of a third-order nonlinear response function (Butcher and Ogg, 1965). The present approach has direct physical appeal, since the linear response functions are related to the dielectric function and determine the modes of the system in a direct way.

TABLE I. Definitions of response functions for simple mechanical and electrical systems.

A. Mechanical	
Displacement	$W(t)=W\exp(-i\omega t)+\mathrm{cc}$ [a]
Force	$F(t)=F\exp(-i\omega t)+\mathrm{cc}$
Energy perturbation	$H'=F(t)W(t)$
Response function	Nyquist's theorem for scattering
$\mathbf{T}(\omega)=W/F$	$\langle \|W\|^2\rangle_\omega=(\hbar/\pi)[n(\omega)+1]\ \mathrm{Im}\ (\mathbf{T})$ $\simeq(k_BT/\pi\omega)\ \mathrm{Im}\ (\mathbf{T})$ at high temperatures
B. Electrical-two terminal network in high temperature limit	
Charge	$Q(t)=Q\exp(-i\omega t)+\mathrm{cc}$
Voltage	$V(t)=V\exp(-i\omega t)+\mathrm{cc}$
Current	$I(t)=I\exp(-i\omega t)+\mathrm{cc}$
Energy perturbation	$H'=Q(t)V(t)$
Response functions[b]	Nyquist's theorem
$\mathbf{T}=Q/V$	$\langle \|Q\|^2\rangle_\omega=(k_BT/\pi\omega)\ \mathrm{Im}\ (\mathbf{T})$
$\mathbf{Y}$(admittance) $=I/V=-i\omega T$	$\langle \|I\|^2\rangle_\omega=(k_BT/\pi)\ \mathrm{Re}\ (\mathbf{Y})$
$\mathbf{Z}$(impedance) $=V/I=1/Y$	$\langle \|V\|^2\rangle_\omega=(k_BT/\pi)\ \mathrm{Re}\ (\mathbf{Z})$

[a] cc means complex conjugate.

[b] Note our convention $\exp(-i\omega t)$ causes the admittance and impedance defined here to be the complex conjugate of the admittance and impedance defined in texts on network theory.

2. TWO-OSCILLATOR MODEL

A. The Equations of Motion

The model we wish to analyze in detail is shown in Fig. 3. To the left side of the figure is the oscillator which is to represent ionic motion. This oscillator consists of the linear spring with restoring force (Hooke's constant) K attached to a particle of mass M. The displacement of the mass from equilibrium is W. In making comparisons with a diatomic crystal, M would be the reduced mass of the two ions in the primitive cell. The oscillator to the right of Fig. 3 represents electronic transitions. A comparison with more detailed shell models shows that the electron restoring force k is the same order of magnitude as K, but the much smaller electronic mass m causes the electronic transitions to occur at a much higher frequency than the ion resonant frequency. The nonlinear spring α couples the two oscillators. It can be thought of as the first correction to a purely quadratic potential. This correction term simulates hard-core repulsion of the ions and electrons in a crystal.

[5] The time derivative results in a factor $i\omega$ in converting from $\mathbf{T}$ to $\mathbf{Z}$ which reverses real and imaginary parts and brings in an additional frequency factor.

[6] The response matrix T_{ij} is analogous to the admittance matrices used in the theory of four-terminal networks (Westman 1961).

To keep all expressions simple and thus emphasize the physical effects, we analyze the model of Fig. 3 as if it were a unit in a cubic crystal. Further, we apply the various driving fields along the bond directions. If we call this the x direction, we will derive diagonal (xx) components of tensors describing various optical effects. We first neglect the nonlinear spring α to derive the linear effects. The equations which define the model are

$$M\ddot{W}=-KW+ZE, \tag{2.1}$$

$$m\ddot{w}=-kw+zE, \tag{2.2}$$

$$P=(ZW+zw)/V, \tag{2.3}$$

where Z and z are the charges of the oscillators which represent the ionic and electronic motions, respectively. Equation (2.3) gives the macroscopic polarization created by the two dipoles, where V is the volume of the primitive cell. E is the macroscopic electric field, thus we are dealing with a *macroscopic* model in the spirit of Born and Huang (1954) who first set up such a model for the lattice vibrations in a diatomic cubic crystal (see Sec. 9 of this reference for a microscopic justification of the macroscopic model).

B. The Linear Dielectric Function

Consider a transverse or longitudinally polarized, oscillating electric field with the field direction along the bond direction in Fig. 3. We take the field to have the form

$$E(t)=E\exp[i(qx-\omega t)]+\text{complex conjugate}. \tag{2.4}$$

We expand all variables in this form and substitute in (2.1) and (2.2) to obtain for the particle response

$$W=ZE/(K-M\omega^2), \qquad w=zE/(k-m\omega^2) \tag{2.5}$$

and the obvious complex conjugate relations for W^* and w^*. Substituting into the polarization equation (2.3) and defining the dielectric function, we obtain

$$\epsilon=1+4\pi(P/E)=1+4\pi(\chi_1+\chi_2), \tag{2.6}$$

where

$$\chi_1=\frac{Z^2/V}{K-M\omega^2}, \tag{2.7}$$

$$\chi_2=\frac{z^2/V}{k-m\omega^2}, \tag{2.8}$$

are the susceptibility functions for the ionic and electronic parts of the system. This dielectric function is independent of q, but has two poles at frequencies given by $\omega^2=K/M$ and k/m. Huang (1951) has shown that there are transverse modes of a mechanical nature at the poles of ϵ. These modes occur only at large values of wave vector q. Longitudinal modes occur at the zeros of ϵ.

The dielectric function ϵ for the present system has two poles and two zeros. Figure 4 shows the frequency response of the particles to a constant-amplitude driving field applied just outside the crystal. Figures 4(a) and 4(b) show the transverse case where resonances occur at the poles of ϵ. Figures 4(c) and 4(d) show the longitudinal case. For this geometry, the normal component of $D=E+4\pi P$ is conserved so that $E(\text{inside})=E(\text{outside})/\epsilon$. This gives an additional $1/\epsilon$ factor in Eqs. (2.5) when they are written in terms of $E(\text{outside})$. The $1/\epsilon$ factor gives resonant response at frequencies where ϵ is zero. We stress that while ϵ and $1/\epsilon$ describe the particle response, some energy is carried by electric and magnetic fields apart from the particles. It is only when we consider Maxwell's equations together with (2.1) to (2.3) that we can obtain the true modes of the system.

To summarize and define some standard notation we write

$$\epsilon=[S_1\omega_1^2/(\omega_1^2-\omega^2)]+[S_2\omega_2^2/(\omega_2^2-\omega^2)]+1, \tag{2.9}$$

where S_1 and S_2 are dimensionless strengths

$$S_1=4\pi Z^2/VK, \qquad S_2=4\pi z^2/Vk, \tag{2.10}$$

and the transverse-mode mechanical resonances are at

$$\omega_1^2=K/M \quad \text{and} \quad \omega_2^2=k/m. \tag{2.11}$$

For $\omega\ll\omega_2$, it is useful to note that

$$\epsilon\simeq[S_1\omega_1^2/(\omega_1^2-\omega^2)]+\epsilon_\infty, \tag{2.12}$$

where

$$\epsilon_\infty=1+(4\pi z^2/Vk) \tag{2.13}$$

is a frequency-independent dielectric constant which ϵ approaches at frequencies well above the ionic resonance ω_1 but well below ω_2. The generalization of (2.9) to include damping and the evaluation of the longitudinal vibration modes has been treated by Barker (1964).

C. The Linear Response to a Mechanical Force

It is now necessary to consider *all* the equations of motion (including Maxwell's equations) in order to derive the response functions needed to evaluate the thermal fluctuations in a dielectric. We must use the

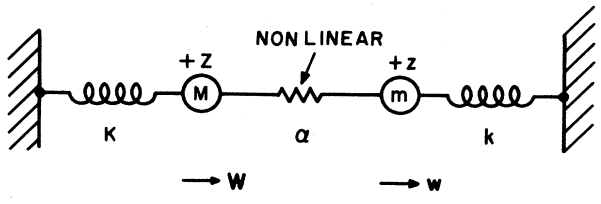

FIG. 3. Two-oscillator model of a dielectric with one vibrational mode. The ion with mass M and charge Z is shown on the left bound by a spring with force constant K. The electron is shown on the right. Here α denotes a purely anharmonic spring coupling the two harmonic systems.

response appropriate to externally applied forces (Landau and Lifshitz, 1962, Sec. 125). In this section we will derive the response function F/W, where F is an external force which drives the ion displacement W. The presence of F adds the energy FW to the system Hamiltonian. The equations of motion must then have the term F added to right side of (2.1). The response function W/F can then be derived and used in Nyquist's theorem to evaluate the fluctuations in the displacement W. If we wish to evaluate the polarization fluctuation, we must consider the energy term PE_{ext}. The response function[7] P/E_{ext} is then used in Nyquist's theorem to obtain $\langle | P |^2 \rangle_\omega$. Alternatively we can drive the system with the external polarization P_{ext}. To obtain the fluctuations in E we must then calculate the response function E/P_{ext}. These latter response functions will be derived in later sections.

For the present, we require the response to a term $F \exp[i(qx-\omega t)]$ added to (2.1). We obtain

$$W=F/(K-M\omega^2). \tag{2.14}$$

According to Maxwell's equations we have

$$\nabla\times\nabla\times\mathbf{E}=-(c^2)^{-1}(\partial^2\mathbf{D}/\partial t^2), \tag{2.15}$$

or equivalently

$$\nabla^2\mathbf{E}-\nabla(\nabla\cdot\mathbf{E})=(c^2)^{-1}(\partial^2/\partial t^2)(\mathbf{E}+4\pi\mathbf{P}). \tag{2.16}$$

Thus with the assumption of transverse plane-wave fields

$$(q/\omega)^2E=E+4\pi P_{\text{tot}}, \tag{2.17}$$

where a factor c representing the velocity of light has been absorbed into q, that is, q is measured in the same units as ω. For the present case, the total polarization is

$$P_{\text{tot}}=\frac{\epsilon-1}{4\pi}E+\frac{ZF/V}{K-M\omega^2}, \tag{2.18}$$

i.e., the usual linear dependence on E plus a new term arising from our external drive on the ion via the force F. Eliminating P_{tot} between (2.17) and (2.18), we obtain

$$E=4\pi ZF/\{V(K-M\omega^2)[(q/\omega)^2-\epsilon]\}. \tag{2.19}$$

The total ion motion is

$$W=\frac{ZE}{K-M\omega^2}+\frac{F}{K-M\omega^2}$$

$$=\left\{\frac{4\pi Z^2}{V(K-M\omega^2)^2[(q/\omega)^2-\epsilon]}+\frac{1}{K-M\omega^2}\right\}F. \tag{2.20}$$

Thus as a result of these calculations we have obtained the response to a mechanical force and find that it has

[7] Note that the dielectric function ϵ is not a response function (except asymptotically for large wave vector). This is because E is not the external field which drives P. Both P/E and P/E_{ext} can be evaluated for our model, but only the latter is to be used in Nyquist's theorem.

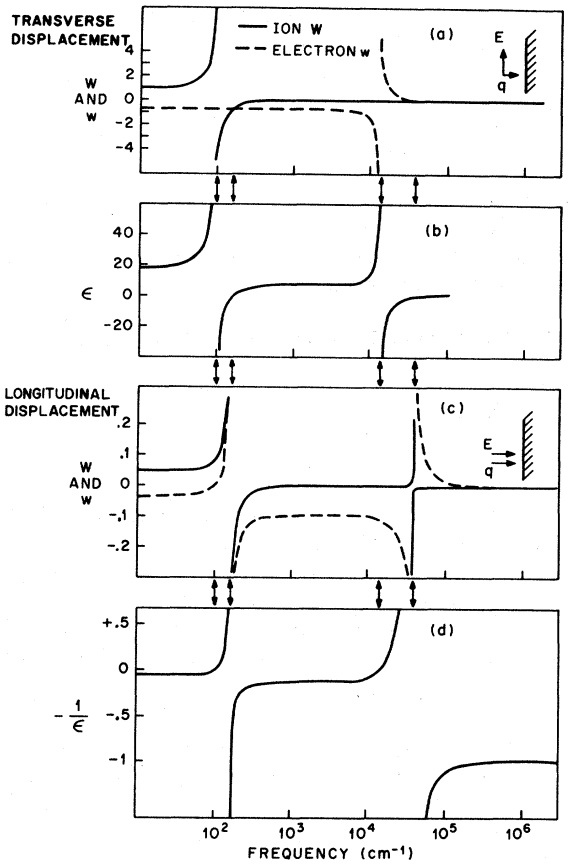

FIG. 4. Particle response and linear dielectric functions for the two-oscillator model. In (a) a transverse electric field is coupled into a slab of the dielectric, (b) shows the dielectric functions. In (c) a longitudinal external field drives the system so that the D field is conserved across the boundary. (d) shows the response function $-1/\epsilon$. The parameters used are $S_1=12.6$, $S_2=6.3$, $\omega_1=100$, $\omega_2=1.41\ 10^4\ \text{cm}^{-1}$ with Z and z having opposite sign. The short vertical arrows mark the transverse and longitudinal resonances in ascending order ω_1, ω_{LO}, ω_2, ω_{LO}.

both frequency and wave-vector dependence for charged oscillators ($Z\neq 0$). If we apply an external driving force to the electron with amplitude f, then by similar methods we obtain the electron response

$$w=\left\{\frac{4\pi z^2}{V(k-m\omega^2)^2[(q/\omega)^2-\epsilon]}+\frac{1}{k-m\omega^2}\right\}F. \tag{2.21}$$

The large brackets in (2.20) and (2.21) contain the admittances or response functions needed to compute the fluctuations of W and w, the ion and electron motion. In addition we will need the fluctuations in the cross term wW. In the language of network theory, we have a four-terminal network, the two variables w and W corresponding to the two currents which can be impressed on the network. Equations (2.20) and (2.21) give us the admittances T_{11} and T_{22} of the four-terminal network. For a complete description we still need $T_{12}=w/F$ since the systems are coupled by Maxwell's equations. The transfer admittance T_{12}

in the present system describes the response of the electron when the ion is driven by F.

Using the same procedures outlined above, we obtain

$$w=\left\{\frac{4\pi zZ}{V(k-m\omega^2)(K-M\omega^2)[(q/\omega)^2-\epsilon]}\right\}F. \quad (2.22)$$

Evaluation of W/f where f is a force driving the electron would have given the same response function in the bracket above, showing that for the present model $T_{12}=T_{21}$, i.e., the admittance matrix is symmetric.

D. The Linear Response–Longitudinal Case

When longitudinal plane wave fields are considered, (2.17) becomes

$$E+4\pi P_{\text{tot}}=0. \quad (2.23)$$

It is apparent that we can retain all the formulae of the above section by letting the term q^2/ω^2 be zero whenever we consider longitudinal waves. In later sections we will see that this result is generally true only for cubic crystals. The response of E to a longitudinal force field applied to the ions is therefore [from Eq. (2.19)]

$$E=4\pi ZF/\{V(K-M\omega^2)(-\epsilon)\}. \quad (2.24)$$

Equations (2.21) and (2.22) can be modified in the same manner for longitudinal fields. The ubiquitous $[(q/\omega)^2-\epsilon]^{-1}$ factor of the transverse case arising from Maxwell's equations has been replaced by the factor $1/(-\epsilon)$. The longitudinal response functions will therefore have peaks at the zeros of ϵ as was anticipated in Sec. 2.B.

All of the linear response functions necessary to describe Raman scattering have now been derived. It is worth stressing that for uncharged particles, only $1/(K-M\omega^2)$ types of response functions would have been obtained. For charged particles, Maxwell's equations must be included in the model causing various combinations of ϵ to appear in the response functions. This coupling of the mechanical and light waves causes new mixed modes in the system called polaritons. The mixed modes are discussed in the next section.

E. The Polariton Modes

In a system capable of oscillations, a mode is generally specified by giving its frequency and in some cases its strength, i.e., its coupling to an external probe. Hopfield (1966) has emphasized that for the case of light waves at frequencies below the x-ray region interacting with a solid, the set of equations which describe the oscillations are Maxwell's equation plus an equation which determines P in terms of E, i.e., an equation for the dielectric function. To gain insight, the equations can be solved separately by ignoring Maxwell's equations while solving (2.1), (2.2), and (2.3), and then solving Maxwell's equation (2.17) with $P_{\text{tot}}=0$, i.e., ignoring the charged oscillators. For our two-oscillator model the resulting uncoupled modes are completely mechanical modes at frequencies ω_1 and ω_2 (Eq. 2.11) and pure electromagnetic modes (light waves) with no dispersion. When the equations are solved together (i.e., simultaneously) as in the previous sections, the resulting coupled modes possess a mixture of mechanical and electromagnetic character. These modes have been named polaritons (Hopfield, 1966).

In the case of any oscillatory system, we may examine the modes by looking at a response function. Going first to the uncoupled case of the ion driven by a force F, we write again (2.14)

$$W=F/(K-M\omega^2).$$

The response function is

$$T\equiv W/F=1/(K-M\omega^2)$$
$$=\frac{\omega_1}{2K}\left(\frac{1}{\omega+\omega_1}-\frac{1}{\omega-\omega_1}\right), \quad (2.25)$$

where ω_1 is defined in (2.11). In conformity with the causality principle (Kittel, 1958), a response function like (2.25) always has an imaginary part which can be determined by associating a small positive imaginary part with ω and taking the limit as this imaginary part tends to zero. Following this procedure for (2.25) we find

$$\text{Im}\,(T)=(\pi\omega_1/2K)[\delta(\omega-\omega_1)-\delta(\omega+\omega_1)]. \quad (2.26)$$

The modes are sharp peaks (delta functions) located at $\pm\omega_1$. When damping is included in the oscillator equation of motion as was done for Fig. 1, the peaks broaden and we have some freedom in choosing the definition of a mode. Obviously the response function **T** contains all the information of interest; however, to plot dispersion curves we must extract one frequency from **T**. We are therefore led to the definition of a mode frequency as the frequency of the peak in the response function.

For polaritons in the model considered in the previous sections, the coupling occurred between the light waves and the transverse mechanical vibrations. The response functions for various particle motions all contained the denominator $[(q/\omega)^2-\epsilon]$. We now *define* the polariton modes as the peaks of

$$\text{Im}\,\{[(q/\omega)^2-\epsilon]\}^{-1}. \quad (2.27)$$

Hopfield in his review article has illustrated the polariton modes in the case of zero damping. In Fig. 5(a) we show $\text{Im}\,[(q/\omega)^2-\epsilon]^{-1}$ for a case of finite damping. In Fig. 5(b) the dispersion curve is plotted from the peaks in Fig. 5(a). In addition, dispersion curves are shown for zero damping and two cases of large damping. In these figures the finite phonon linewidth has been generated by addition of a damping term $M\Gamma\dot{W}$ to the right-hand side of (2.1).

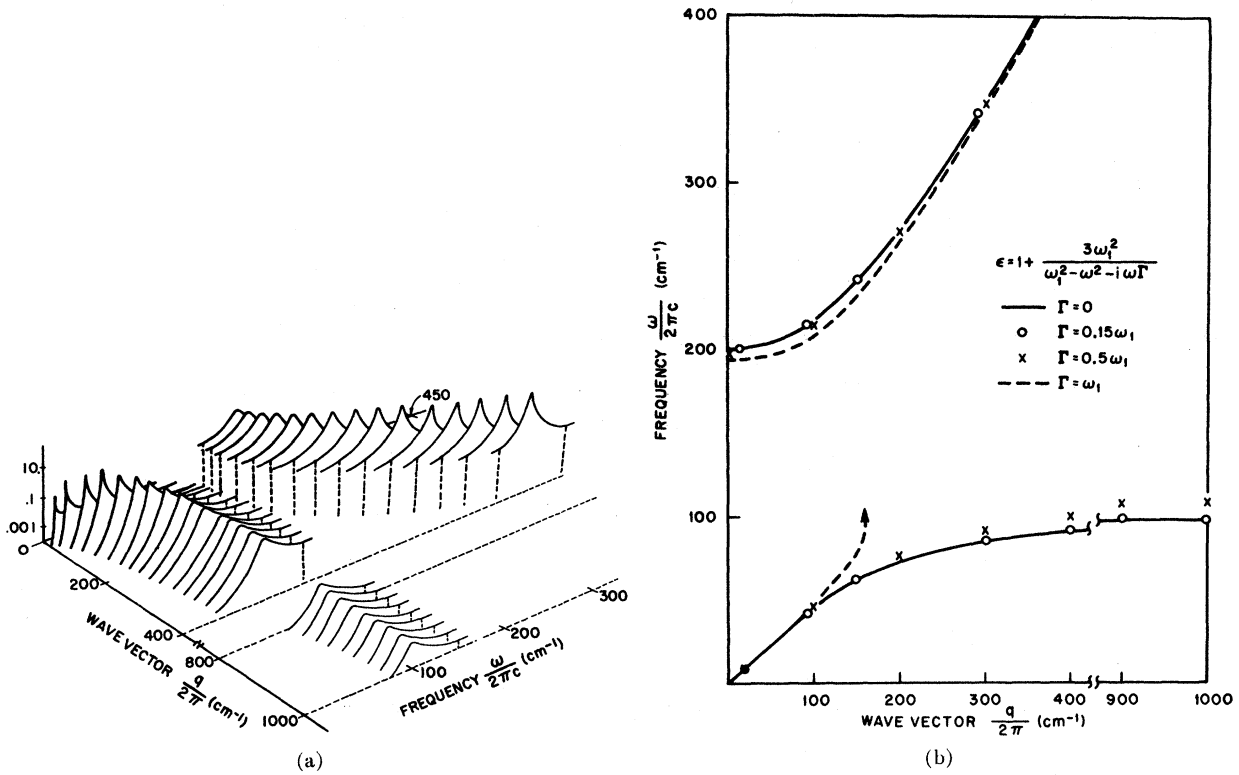

FIG. 5. (a) Polariton response function $\mathrm{Im}[(q/\omega)^2-\epsilon]^{-1}$. The spectrum has been plotted in the region of the lattice vibration using the two-oscillator model with parameters $S=3$, $\omega_1=100$ cm^{-1}, $\Gamma=0.15\omega_1$, $\epsilon_\infty=1$. The peaks clearly show the transition from light waves to damped lattice vibrational waves. Note that the vertical scale is logarithmic and some portions of contours have been omitted for clarity. (b) Polariton dispersion curves for several choices of damping. The open circles correspond to the peak positions shown in Fig. 5(a). The dashed curve corresponds to very large damping such that the response function shows no peak but only a broad shoulder near $\omega=100^{-1}$ for $q/2\pi>150$ cm^{-1}.

For longitudinal vibrations, (2.27) becomes Im $(1/-\epsilon)$ and the peaks show no dispersion. In this case, there is no coupling of the mechanical and light waves and the term polariton is inappropriate. Figure 6(b) shows a longitudinal spectrum.

One point needs further emphasis. While the definition of a mode as the imaginary part of some response function is obviously useful and certainly pictorial, the particular response function chosen is somewhat arbitrary. The definition (2.27) is a fairly natural one but the result of a particular experiment may involve a different response function. For Raman scattering, the function (2.27) is in fact multiplied by another function which for a certain choice of parameters and at a certain value of q can have a dip right at the peak in (2.27). The resulting Raman scattering may therefore have no peak at the polariton mode. It is incorrect to say that there is no polariton mode, however, since some other probe (e.g., neutron scattering) with a different response function would show a peak here. The definition (2.27) contains the universal factor which appears in any more complicated response function and is thus particularly useful as a definition.

F. Nonlinear Effects–The Electrooptic Coefficient

The nonlinear spring in Fig. 3 is regarded as contributing an anharmonic term $(\alpha/3)(W-w)^3$ to the potential energy of the system. Its inclusion changes the equations of motion to

$$M\ddot{W}=-KW-\alpha(W-w)^2+ZE \qquad (2.28)$$

$$m\ddot{w}=-kw+\alpha(W-w)^2+zE \qquad (2.29)$$

$$P=(ZW+zw)/V. \qquad (2.30)$$

For the electro-optic effect we consider the case of two electric fields driving the system. We may think of one field (the "optic" field) as resulting from a laser

$$E_l(t)=E_l\exp(-i\omega_l t)+E_l^*\exp(i\omega_l t) \qquad (2.31)$$

and the second (the "electro" field) as resulting from a source with frequency ω low compared with the frequencies of the resonances in the system, i.e.,

$$E(t)=E\exp(-i\omega t)+\text{cc}. \qquad (2.32)$$

With these definitions the peak fields are $2\,|E_l|$ and $2\,|E|$, respectively.

The linear response of the ion is

$$W=[ZE\exp(-i\omega t)/(K-M\omega^2)]+[ZE_l\exp(-i\omega_l t)/(K-M\omega_l^2)]+\text{cc} \quad (2.33)$$

and a similar expression for w, the electron motion. Inserting these expressions into the nonlinear terms in (2.28) and (2.29), we find that W and w have terms vibrating at zero frequency, and at double the applied frequencies, as well as at $\omega_l\pm\omega$. We use the term "scattered frequency" to denote this latter combination. We deal specifically with the "down-shifted frequency"

$$\omega_s=\omega_l-\omega, \quad (2.34)$$

and find for the displacements at this frequency

$$W(\omega_s)=-\frac{2\alpha}{K-M\omega_s^2}\left\{\frac{ZE^*}{K-M\omega^2}-\frac{zE^*}{k-m\omega^2}\right\}\times\left\{\frac{ZE_l}{K-M\omega_l^2}-\frac{zE_l}{k-m\omega_l^2}\right\}, \quad (2.35)$$

$$w(\omega_s)=\frac{2\alpha}{k-m\omega_s^2}\left\{\frac{ZE^*}{K-M\omega^2}-\frac{zE^*}{k-m\omega^2}\right\}\times\left\{\frac{ZE_l}{K-M\omega_l^2}-\frac{zE_l}{k-m\omega_l^2}\right\}. \quad (2.36)$$

The relative importance of the various terms which result from multiplying out these equations depends on the magnitudes of the three frequencies which enter, and will be different for different nonlinear-optical processes. For the electro-optic effect, ω_l and ω_s are close in magnitude and are very much larger than $(K/M)^{1/2}$ and the third frequency ω. It follows that $w(\omega_s)$ is much larger than $W(\omega_s)$ and that the first term in the second bracket of (2.36) is much smaller than the second. Thus to a good approximation

$$w(\omega_s)=\frac{2\alpha zE^*E_l}{(k-m\omega_s^2)(k-m\omega_l^2)}\times\left\{\frac{z}{k-m\omega^2}-\frac{Z}{K-M\omega^2}\right\}, \quad (2.37)$$

and $W(\omega_s)$ can be ignored.

The nonlinear polarization vibrating at ω_s is obtained by substituting (2.37) into (2.30)

$$P_{NL}(\omega_s)=\frac{2z^2\alpha}{V(k-m\omega_s^2)(k-m\omega_l^2)}\times\left\{\frac{z}{(k-m\omega^2)}-\frac{Z}{(K-M\omega^2)}\right\}E^*E_l. \quad (2.38)$$

For the "up-shifted" frequency we have $\omega_s=\omega_l+\omega$ and the electric fields at the right-hand side become EE_l. The entire coefficient of E^*E_l is a second-order susceptibility describing the electro-optic effect. It may be related to first-order susceptibilities as Garrett (1968) has done, by using the quantities χ_1 and χ_2 defined in (2.7) and (2.8),

$$P_{NL}(\omega_s)=\frac{2\alpha V^2\chi_2(\omega_s)\chi_2(\omega_l)}{z^2}\times\left\{\frac{\chi_2(\omega)}{z}-\frac{\chi_1(\omega)}{Z}\right\}E^*E_l. \quad (2.39)$$

The nonlinear coefficient of E^*E_l in (2.38) or (2.39) is equivalent to $4d$ in the notation of Boyd and Kleinman (1968). We note that there are two terms and that there can be cancellation between them. Zero electro-optic effect will result if Z and z have appropriate sign and magnitude to cause cancellation inside the bracket. We will find cancellations of a similar nature in the Raman response.

The two terms entering the bracket in (2.38) are associated with electronic and ionic contributions to the electro-optic effect. The ionic contribution will be zero for an infrared inactive mode ($Z=0$). The formal electro-optic coefficient, r, is defined in terms of the derivative of the reciprocal of the susceptibility with respect to the low-frequency electric field (Kaminow, 1967). Using cgs units, we write:

$$r=\frac{\partial(1/\epsilon)}{\partial E^*}=\frac{-1}{\epsilon^2}\frac{\partial\epsilon}{\partial E^*}=\frac{-4\pi}{\epsilon^2}\frac{\partial(P_{NL}/E_l)}{\partial E^*}. \quad (2.40)$$

For the present one-dimensional model, the coefficient is

$$r=\frac{-8\pi z^2\alpha}{\epsilon^2V(k-m\omega_s^2)(k-m\omega_l^2)}\times\left(\frac{z}{(k-m\omega^2)}-\frac{Z}{(K-M\omega^2)}\right), \quad (2.41)$$

where ϵ is the dielectric function evaluated at the laser frequency.

In many cases, all of the frequency dependent denominators in (2.38) and (2.41) are far from resonance and can be replaced by constants. We can make contact with much of the current literature on nonlinear optics by defining the coefficients

$$a=-2z^2\alpha/[V(k-m\omega_s^2)(k-m\omega_l^2)] \quad (2.42)$$

$$b=2z^3\alpha/[V(k-m\omega_s^2)(k-m\omega_l^2)(k-m\omega^2)]. \quad (2.43)$$

The nonlinear polarization equation (2.38) then simplifies to

$$P_{NL}(\omega_s)=aW^*E_l+bE^*E_l, \quad (2.44)$$

where W is the amplitude of the ion motion at the frequency ω. Equation (2.44) clearly shows that the coefficients a and b describe the ion and electric-field contributions to the electro-optic effect. Many discussions of electro-optic effect and light scattering intensities break up the nonlinear polarization in this way (Johnston and Kaminow, 1969; Johnston, 1970; Burstein and Mills, 1969*a*, *b*) so that the parameters a and b are taken as basic model parameters. Equations

(2.42) and (2.43) show that the two-oscillator model gives the same results, and in addition can be used to describe resonant effects when ω_l or ω_s approach the electronic transition frequency. In terms of the a and b coefficients, the electro-optic coefficient is

$$r=(-4\pi/\epsilon^2)\{a[Z/(K-M\omega^2)]+b\}, \quad (2.45)$$

where we have made use of the derivative rule

$$\partial/\partial E^*=(\partial W^*/\partial E^*)(\partial/\partial W^*).$$

G. Nonlinear Effects–Raman Scattering

We now consider the case where a laser field is impressed on the model and in addition the electron and ion vibrate thermally at the frequency ω. While we think of ω as a phonon frequency, it is retained as a variable. At the end of the calculation the scattering spectrum is examined as a function of ω. There will be peaks when ω is near phonon (or polariton) frequencies.

The calculation proceeds much as in the case of the electro-optic effect. The linear fields present are the laser $E_l \exp i(q_l x-\omega_l t)$, and the particle vibrations $W \exp i(qx-\omega t)$ and $w \exp i(qx-\omega t)$. All of the amplitudes E_l, W, and w can be thought of initially as driving the system to produce the nonlinear response at $\omega_s=\omega_l-\omega$, $q_s=q_l-q$. Here W and w are thermally driven however, so finally we must calculate the *power* spectrum using Nyquist's theorem for the fluctuation in W and w.

We begin with the laser field at frequency ω_l and the particle vibrations at frequency ω with amplitude $W(\omega)$ and $w(\omega)$. For compactness, we cease writing the complex conjugate terms for each field,

laser

$$E_l \exp(-i\omega_l t), \quad (2.46)$$

ion motion

$$W(\omega) \exp(-i\omega t)+\frac{ZE_l \exp(-i\omega_l t)}{K-M\omega_l^2}, \quad (2.47)$$

electron motion

$$w(\omega) \exp(-i\omega t)+\frac{zE_l \exp(-i\omega_l t)}{k-m\omega_l^2}. \quad (2.48)$$

Inserting into the equations of motion (2.28) and (2.29), we obtain, as before, frequency doubling, rectification, and frequency mixing from the nonlinear term. Considering only the mixing process, and writing out only the down-shifted or Stokes contributions, the electron motion at $\omega_s=\omega_l-\omega$ has wave vector q_l-q, and amplitude

$$w(\omega_s)=\frac{2\alpha}{k-m\omega_s^2}[W^*(\omega)-w^*(\omega)] \times\left(\frac{ZE_l}{K-M\omega_l^2}-\frac{zE_l}{k-m\omega_l^2}\right). \quad (2.49)$$

A similar expression is obtained for $W(\omega_s)$; however the prefactor of $\alpha/(K-M\omega_s^2)$ makes the ion amplitude negligibly small under the usual conditions of Raman scattering. For the same reasons, (because $M\gg m$) the first term in the large bracket above can be neglected. Inserting (2.49) in the polarization equation (2.30), and neglecting small terms the nonlinear polarization vibrating at the scattered frequency ω_s is:

$$P_{NL}(\omega_s)=\frac{2\alpha z^2}{V}[w^*(\omega)-W^*(\omega)] \times\frac{E_l}{(k-m\omega_s^2)(k-m\omega_l^2)}. \quad (2.50)$$

Equation (2.50) shows a number of features to be expected of the Raman effect. The nonlinear parameter α enters as well as the electronic charge squared. The electron and ion amplitudes enter linearly. At some frequency, for a suitable choice of parameters, W and w may vibrate in phase, giving zero Raman scattering. Finally there is a resonant enhancement of the Raman scattering when either the scattered frequency ω_s or the laser frequency ω_l approach the electronic resonant frequency $(k/m)^{1/2}$.

Before defining the Raman scattering cross section, we examine the fluctuations in $P_{NL}(\omega_s)$ which have essentially the same spectrum. The power spectrum of the nonlinear polarization, which we now call the Raman polarization, is

$$\frac{\langle|P_{NL}|^2\rangle_{\omega_s}}{|E_l|^2}=\frac{4\alpha^2 z^4}{V^2(k-m\omega_s^2)^2(k-m\omega_l^2)^2} \times\langle|w(\omega)-W(\omega)|^2\rangle_\omega. \quad (2.51)$$

Using Nyquist's theorem (1.1) first on $\langle|W(\omega)|^2\rangle$, we obtain for transverse vibrations using (2.20)

$$\langle|W|^2\rangle_\omega=(\hbar/\pi)[n(\omega)+1] \times \mathrm{Im}\left(\frac{4\pi Z^2}{V(K-M\omega^2)^2[(q/\omega)^2-\epsilon]}+\frac{1}{K-M\omega^2}\right). \quad (2.52)$$

Using (2.21) and (2.22) to obtain $\langle|w|^2\rangle_\omega$ and $\langle Ww^*\rangle_\omega$, the power spectrum of the Raman polarization at frequency ω_s and wave vector q_s is

$$\frac{\langle|P_{NL}|^2\rangle_{\omega_s}}{|E_l|^2}=\frac{4\alpha^2 z^4\hbar[n(\omega)+1]/\pi}{V^2(k-m\omega_s^2)^2(k-m\omega_l^2)^2} \mathrm{Im}\left\{\frac{4\pi Z^2}{V(K-M\omega^2)^2[(q/\omega)^2-\epsilon]} +\frac{1}{K-M\omega^2}+\frac{4\pi z^2}{V(k-m\omega^2)^2[(q/\omega)^2-\epsilon]}-\frac{8\pi zZ}{V(K-M\omega^2)(k-m\omega^2)[(q/\omega)^2-\epsilon]}\right\}. \quad (2.53)$$

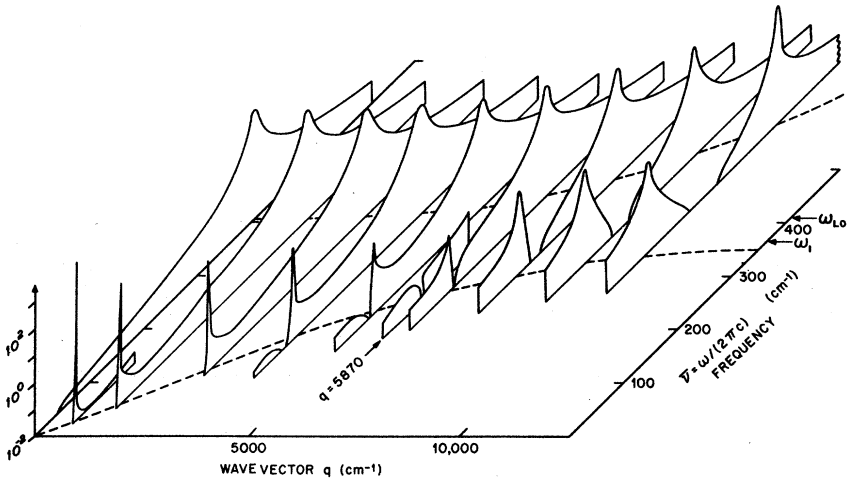

(a)

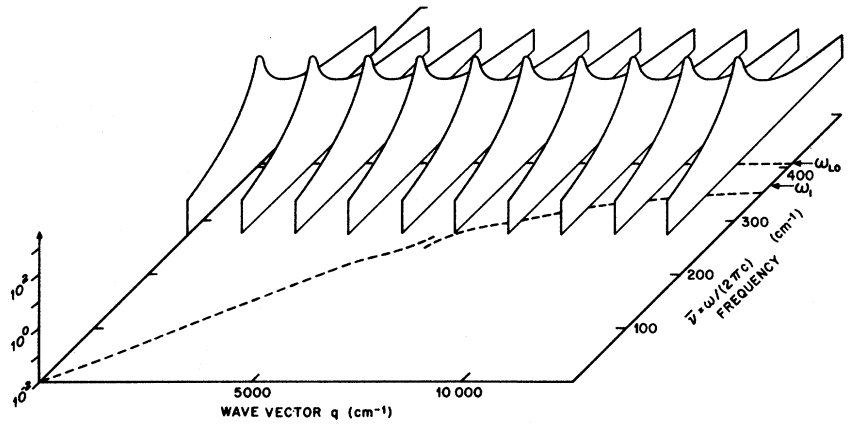

(b)

FIG. 6. (a) Response function for Raman scattering for transverse vibrations (parameters given in Table II). The thermal factor is omitted. The vertical axis is logarithmic and only values greater than 10^{-2} are plotted. Note the disappearance of the lower peak at $q=5870$ cm^{-1}. The dashed curves give the location of the peaks. (b) Response function for Raman scattering by logitudinal vibrations (parameters given in Table II). The lower frequency dashed curve gives the peak position for transverse scattering shown in Fig. 6(a). It clearly shows the dispersion near the interference which causes cancellation near $q=5870$ cm^{-1}. The higher frequency dashed curve gives the frequency of the peak of the longitudinal mode and is a straight line.

To obtain some feeling for the power spectrum of P_{NL}, we study the nonresonant case. Indeed we shall assume nonresonant conditions for most of the paper, and give special attention to the resonant case in Sec. 4.E.

Figures 6 and 7 show some spectra as functions of q and ω. Phonon damping has been included as in Fig. 5. A similar damping could be included in the electron equation of motion, but such a modification is important only when resonant effects are considered and would not influence Figs. 6 and 7. Table II lists the parameters used in the figures. The phonon frequencies have been chosen to approximate GaP. The peaks in $\langle|P_{NL}|^2\rangle$ closely follow the polariton dispersion curve, however there are significant small shifts. In Fig. 6, Z/z is positive. It is easy to show that for this sign choice there is always a frequency where the Raman scattering has zero intensity in the range $0<\omega<\omega_1$ [8] as long as $(Z/z)(\epsilon_\infty-1)+\epsilon_\infty$ is larger than $\epsilon_0-\epsilon_\infty$. In Fig. 6 this cancellation effect occurs at $\omega=259$ cm^{-1}. Measurements by Faust *et al.* (1968) on GaP show a cancellation at this frequency. As emphasized in Sec. 2.E, the polariton mode dispersion curve still exists and passes smoothly through $\omega=259$ cm^{-1}, while the peaks in $\langle|P_{NL}|^2\rangle$ actually show a discontinuity here as shown by the dashed line in Fig. 6(b). In Fig. 6(b), the spectrum is shown for longitudinal phonon fluctuations. In Fig. 7, Z/z is chosen negative, giving a cancellation in the scattering above ω_{LO} at $\omega=448$ cm^{-1}. Roughly speaking, a cancellation either above ω_{LO} or below ω_1 is to be expected when ϵ_∞ is large compared with S_1, the phonon mode strength.

The scattering cross section is obtained by considering the radiation emitted by the oscillating dipole $P_{NL}(\omega_s)$. At a point situated a large distance R and oriented at right angles to the direction of P_{NL}, the time average power flow per unit area is

$$I_s=\frac{V^2}{2\pi c^3R^2}\int_{-\infty}^{\infty}n_s\omega_s^4\langle|P|^2\rangle_{\omega_s}\,d\omega_s. \qquad (2.54)$$

[8] We continue to use ω_1 for the frequency of the resonance in ϵ. ω_1 is the same as the transverse optic frequency (usually denoted ω_{TO}) for zero damping. For finite damping a suitably defined response function peaks at ω_1 so that we can consistently define ω_1 to be the transverse optic-mode frequency in all cases.

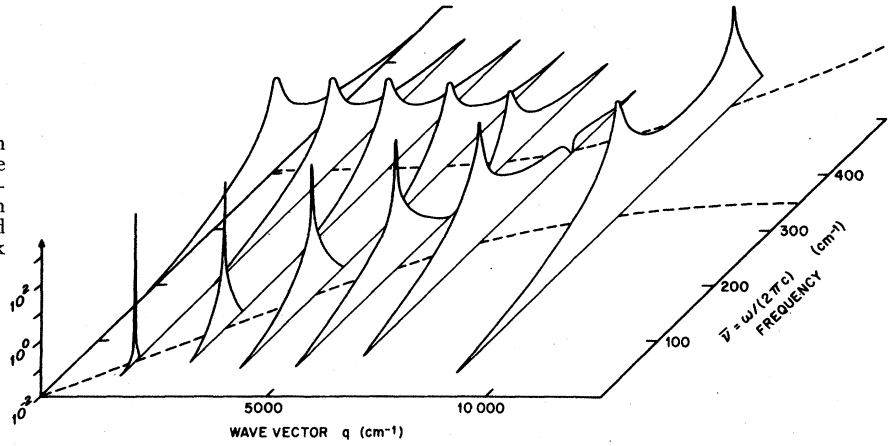

FIG. 7. Response function for Raman scattering by transverse vibrations. The parameters used (Table II) give a cancellation in the higher frequency polariton branch near $q=6000$ cm^{-1}. The dashed curves give the frequency of the peak in the response function.

Here cgs units have been used. V is the unit cell volume associated with the polarization [Eq. (2.3)], and n_s is the index of refraction at the scattered frequency ω_s. Equation (2.54) is just the standard textbook result for the time-averaged Poynting vector associated with an oscillating electric dipole. The time-averaged power flow per unit area for the laser beam is

$$I_l=(cn_l/2\pi)\mid E_l^2\mid, \tag{2.55}$$

where n_l is the index of refraction at the laser frequency ω_l.

The scattering cross section σ is defined as the energy removed from the laser beam per unit time divided by the power flow I_l for the laser beam,

$$\sigma=(\omega_l/\omega_s I_l)\int I_s R^2 d\Omega, \tag{2.56}$$

where $d\Omega$ is an element of solid angle, and the integral runs over a sphere. The factor ω_l/ω_s takes account of the fact that each quantum $\hbar\omega_l$ removed from the laser beam generates a scattered quantum of smaller energy $\hbar\omega_s$, the balance of energy being given to the scattering material.

The differential cross section can be evaluated from (2.54), (2.55), and (2.56)

$$d^2\sigma/d\Omega d\omega_s=(n_s\omega_s^3\omega_l V^2\langle\mid P\mid^2\rangle_{\omega_s})/(n_l c^4\mid E_l\mid^2). \tag{2.57}$$

Except for the weak frequency dependence ω_s^3 and possible resonance of ω_s with the electronic transition which may cause n_s to have some significant frequency dependence, the cross section has the same spectrum as the Raman polarization and will show the peaks illustrated in Figs. 6 and 7.

We make one further simplification of the Raman scattering formulas by restricting ω to lie well below the electron resonance. This allows the neglect of $m\omega^2$ compared with k, and the replacement of certain combinations of parameters by ϵ_∞. From (2.12), (2.13), (2.53), and (2.57), we obtain for scattering by transverse waves

$$\frac{d^2\sigma}{d\Omega d\omega_s}=\frac{n_s\omega_s^3\omega_l V(2\alpha)^2 z^4\hbar[n(\omega)+1]}{n_l c^4(k-m\omega_s^2)^2(k-m\omega_l^2)^2 4\pi^2 Z^2}\,\mathrm{Im}\left(\frac{(\epsilon-\epsilon_\infty)[(q/\omega)^2-\epsilon_\infty-2(Z/z)(\epsilon_\infty-1)]+(Z/z)^2(\epsilon_\infty-1)^2}{(q/\omega)^2-\epsilon}\right), \tag{2.58}$$

where $\omega_s=\omega_l-\omega$.

In (2.58) all of the ion resonance terms have been rewritten in terms of the dielectric function ϵ. The most important terms which determine the spectral response are contained in the large bracket. The denominator $(q/\omega)^2-\epsilon$ causes the response to peak generally near the polariton dispersion curve (Sec. 2.E). The effect of various choices of Z/z in the numerator can strongly affect the spectrum in certain regions, however, as was illustrated in Figs. 6 and 7. Equation (2.58) is the final result giving the Raman cross section for any q and ω in terms of the parameters of the two-oscillator model.

3. GENERALIZATION TO MULTIATOMIC, NONISOTROPIC CRYSTALS

A. Equation of Motion and Linear Dielectric Functions

The theory of Sec. 2 can be generalized in a straightforward way to embrace more complicated crystals, where there may be many vibrational degrees of freedom and where the optical symmetry may be uniaxial or orthorhombic. The inclusion of such complexities in the theory is the purpose of the present section. The results will be qualitatively similar to those for an optically isotropic crystal having a single

TABLE II. Model parameters used to calculate Raman scattering response functions.

	S_1	ω_1	Γ_1/ω_1	Z/z	ϵ_∞
Fig. 6(a), (b)[a]	2	366	0.03	0.5	9
Fig. 7	2	366	0.03	−0.5	9

[a] These parameters approximate gallium phosphide but with slightly increased damping for convenience in drawing the peaks.

vibrational degree of freedom, but the corresponding expressions will look more complicated due to the necessity of enumerating vibrational degrees of freedom and crystal principal axis directions. Damping of the lattice vibrations will also be included.

Consider a crystal having optic vibrational modes enumerated by a superscript ν, the vibrational amplitudes being $\mathbf{W}^\nu$. For a polar optic mode ν, the vibrational amplitude $\mathbf{W}^\nu$ can be assigned to one of the principal axes j of the dielectric tensor. We denote the appropriate element of the diagonalized dielectric tensor ϵ_j, and we also attach a label j to the vibrational amplitude to indicate its principal axis direction. The classical oscillator equation of motion for $W_j{}^\nu$ is obtained by generalizing (2.1) to

$$M_\nu[\ddot{W}_j{}^\nu+\Gamma_\nu\dot{W}_j{}^\nu+\omega_\nu{}^2W_j{}^\nu]=Z_\nu E_j, \tag{3.1}$$

where E_j is the component of the macroscopic electric field along principal axis j, M_ν is the appropriate reduced ionic mass, Γ_ν is the damping constant, ω_ν is the natural frequency, and Z_ν is the effective charge. These latter four parameters have different values for the different normal modes ν.

The total polarization component is a sum of ionic and electronic contributions as in (2.13)

$$P_j=P_j{}^{\text{ionic}}+P_j{}^{\text{electronic}}, \tag{3.2}$$

where

$$P_j{}^{\text{ionic}}=\sum_\nu (Z_\nu W_j{}^\nu/V). \tag{3.3}$$

For the calculations of the present section, we do not set up any microscopic model for the electronic states of the crystal. We assume the electronic resonances to be well separated from the ionic resonances so that the electronic contribution to the dielectric function has a constant value $\epsilon_{j\infty}$ in the ionic resonance region. The electronic polarization at frequencies in the vicinity of the ionic resonances can then be represented as

$$P_j{}^{\text{electronic}}=[(\epsilon_{j\infty}-1)/4\pi]E_j. \tag{3.4}$$

By definition of the dielectric function ϵ_j, the principal axis components of $\mathbf{P}$ and $\mathbf{E}$ are related by

$$E_j+4\pi P_j=\epsilon_j E_j \tag{3.5}$$

where the restriction to orthorhombic or higher symmetry crystals ensures that the dielectric tensor is diagonal allowing the single subscript form ϵ_j to be used. We consider only harmonic plane-wave excitations in the crystal for which $\mathbf{E}$, $\mathbf{P}$, and $\mathbf{W}$ have space and time dependence $\exp[i(\mathbf{q}\cdot\mathbf{r}-\omega t)]$. Elimination of E_j, P_j, and $W_j{}^\nu$ from (3.1), (3.2), and (3.5) then gives

$$\epsilon_j=\epsilon_{j\infty}+\sum_\nu S_\nu\omega_\nu{}^2/(\omega_\nu{}^2-\omega^2-i\omega\Gamma_\nu), \tag{3.6}$$

where

$$S_\nu=4\pi Z_\nu{}^2/VM_\nu\omega_\nu{}^2. \tag{3.7}$$

These are the generalizations of (2.10) and (2.12).

Any excitation set up in the crystal must have $\mathbf{E}$ and $\mathbf{P}$ vectors which are consistent with Maxwell's equations (2.16). This imposes a condition on $\mathbf{E}$ and $\mathbf{P}$ which can be written in either of the equivalent forms

$$\mathbf{E}=-4\pi[\mathbf{q}(\mathbf{q}\cdot\mathbf{P})-\omega^2\mathbf{P}]/(q^2-\omega^2) \tag{3.8}$$

or

$$4\pi\omega^2\mathbf{P}=(q^2-\omega^2)\mathbf{E}-\mathbf{q}(\mathbf{q}\cdot\mathbf{E}), \tag{3.9}$$

where factors of c which multiply q everywhere have been absorbed into q as was done in Sec. 2.C. The last equation reduces to (2.17) for a transverse excitation. The three components each of $\mathbf{E}$ and $\mathbf{P}$ can be eliminated from (3.5) and (3.8) or (3.9). The resulting relations between q, ω, and the ϵ_j determine the polariton dispersion curves. We do not follow this procedure here, but will obtain the polariton dispersion relations as the denominators of response functions, as in Sec. 2.E.

B. The Linear Response to an Applied Electrical Polarization

The nonlinear effects to be considered require a knowledge of the fluctuations in the $W_j{}^\nu$ and the components of $\mathbf{E}$, and also of cross correlations between $W_j{}^\nu$ and $\mathbf{E}$. In this and the following section we derive the response functions or admittances needed to evaluate the magnitudes of these fluctuations.

For the fluctuations which involve $\mathbf{E}$, we require the electric-field response to an external stimulus. The appropriate stimulus which couples to $\mathbf{E}$ is an impressed polarization $\mathbf{P}^{\text{ext}}$, taken to have space and time dependence $\exp[i(\mathbf{q}\cdot\mathbf{r}-\omega t)]$. In addition to $\mathbf{P}^{\text{ext}}$, there will be an electric field $\mathbf{E}$ in the crystal, and an associated induced polarization $\mathbf{P}$ related to $\mathbf{E}$ by (3.5). The polarization in Maxwell's equations must now be taken as the total $\mathbf{P}+\mathbf{P}^{\text{ext}}$. We substitute this in (3.9) to obtain

$$4\pi\omega^2(\mathbf{P}+\mathbf{P}^{\text{ext}})=(q^2-\omega^2)\mathbf{E}-\mathbf{q}(\mathbf{q}\cdot\mathbf{E}). \tag{3.10}$$

Take a principal-axis component and use (3.5) to eliminate P_j,

$$4\pi\omega^2P_j{}^{\text{ext}}=(q^2-\epsilon_j\omega^2)E_j-q_j(\mathbf{q}\cdot\mathbf{E}). \tag{3.11}$$

We define the electric-field response function

$$T_{ij}=E_i/VP_j{}^{\text{ext}}. \tag{3.12}$$

The T_{ij} can be determined by orienting $\mathbf{P}^{\text{ext}}$ parallel to principal axis j. The three principal-axis components of (3.10) then give (3.11) for the j component, and two equations for the remaining components which are similar to (3.11) on the right but have zeros on the left-hand sides. The resulting three simultaneous equations for T_{ij} ($i=1, 2, 3$) can be solved easily by determinantal methods. We use 1, 2, and 3 as labels for the principal-axis directions, and continue to exclude monoclinic and triclinic crystals so that only three dielectric functions (ϵ_1, ϵ_2, and ϵ_3) occur in what follows.

It is simplest to give results for typical diagonal and off-diagonal components of the response function,

$$T_{11}=-(4\pi/VD)\{q^2q_1^2 -[\epsilon_2(q_1^2+q_2^2)+\epsilon_3(q_1^2+q_3^2)]\omega^2+\epsilon_2\epsilon_3\omega^4\}, \quad (3.13)$$

$$T_{21}=-(4\pi/VD)q_2q_1(q^2-\epsilon_3\omega^2)=T_{12}, \quad (3.14)$$

where

$$D=q^2(\epsilon_1q_1^2+\epsilon_2q_2^2+\epsilon_3q_3^2) -[\epsilon_1(\epsilon_2+\epsilon_3)q_1^2+\epsilon_2(\epsilon_3+\epsilon_1)q_2^2 +\epsilon_3(\epsilon_1+\epsilon_2)q_3^2]\omega^2+\epsilon_1\epsilon_2\epsilon_3\omega^4. \quad (3.15)$$

The four other admittances all contain the same denominator D. They can be obtained by cyclic permutation of the subscripts in (3.13) and (3.14). Here T is symmetric as shown by (3.14).

As discussed in Sec. 2.E, the poles of the response functions determine the polariton dispersion curves. The ω versus q relation for the polaritons is obtained by finding the peaks of Im $(1/D)$. This result is slightly more than just a generalization of (2.27) since transverse, longitudinal, and mixed-polarization modes are included in the response function here. It was shown in Sec. 2.E that for moderate damping the peaks of the response function lie close to the peak positions in the limit of zero damping, where the condition for a peak is simply

$$D=0 \qquad \text{(zero damping)}. \quad (3.16)$$

Substituting D from (3.15), the dispersion curves appropriate to an orthorhombic crystal are obtained. We may specialize (3.15) to uniaxial or cubic crystals to compare with results previously derived by other authors for the zero damping case. The orthorhombic case is further discussed in Sec. 4. For a uniaxial crystal having 3 as the unique axis, we set

$$\epsilon_1=\epsilon_2, \quad (3.17)$$

and the denominator factorizes

$$D=(q^2-\epsilon_1\omega^2)[\epsilon_1(q_1^2+q_2^2)+\epsilon_3q_3^2-\epsilon_1\epsilon_3\omega^2]. \quad (3.18)$$

The admittances have poles at

$$q^2=\epsilon_1\omega^2, \quad (3.19)$$

which is the dispersion relation for the ordinary polaritons, and at

$$\epsilon_1(q_1^2+q_2^2)+\epsilon_3q_3^2=\epsilon_1\epsilon_3\omega^2, \quad (3.20)$$

which is the dispersion relation for the extraordinary polaritons. These results have been given previously by Loudon (1964).

For a cubic or isotropic crystal we set

$$\epsilon_1=\epsilon_2=\epsilon_3=\epsilon, \quad (3.21)$$

and the denominator reduces to

$$D=\epsilon(q^2-\epsilon\omega^2)^2. \quad (3.22)$$

The admittances now have poles at

$$\epsilon=0, \quad (3.23)$$

corresponding to the longitudinal mode frequencies, and double poles at

$$q^2=\epsilon\omega^2, \quad (3.24)$$

corresponding to the doubly degenerate transverse polariton branches. Huang (1951) and Born and Huang (1954) have given the above results for the cubic case. The above results also agree with (2.27) and the result for the longitudinal case given in the discussion in Sec. 2.E.

The polariton degeneracies are usually smaller than the crystal symmetry group theory would predict, as mentioned in the introduction. For example, in cubic crystals, group theory predicts that an electric-dipole active excitation should have a threefold degeneracy, whereas the results of the previous paragraph show the polariton branches to be at most doubly degenerate. An exception to this statement occurs for very long-wavelength polaritons when $q\ll\omega$ and the pairs of transverse poles from (3.24) coalesce with single poles from (3.23) to produce threefold degeneracies at $q=0$. Indeed, the group-theory prediction applies rigorously only at $q=0$, so that strictly there is no discrepancy between group theory and the polariton theory given above. The apparent discrepancy arises because the group-theoretical degeneracy is lifted as soon as q becomes of order ω. This occurs for polariton wavelengths λ which are still about five orders of magnitude larger than the crystal lattice spacing a. It is important to realize that for problems involving interactions with the electromagnetic field, the validity of $q=0$ group theory depends on $\lambda\gg a$ *and* $\lambda\gg c/\omega$. A similar state of affairs holds in uniaxial crystals where some branches are two-fold degenerate at $q=0$ in agreement with group theory, this degeneracy being lifted except for propagation parallel to the c-axis as q is increased.

The general forms (3.13) and (3.14) of the admittances simplify sufficiently in the cubic case for the different admittance components to be expressed in a single formula

$$T_{ij}=-(4\pi/V)[(q_iq_j-\epsilon\omega^2\delta_{ij})/\epsilon(q^2-\epsilon\omega^2)]. \quad (3.25)$$

TABLE III. Response functions for an isotropic dielectric.[a]

Energy perturbation	Response function T for Transverse wave	Longitudinal wave
$H'=P_{ext}EV$	$E/VP_{ext}=[(4\pi/V)/(q^2/\omega^2-\epsilon)]$	$E/VP_{ext}=-4\pi/V\epsilon$
$H'=E_{ext}PV$	$E/E_{ext}=[(\epsilon-1)/(q^2/\omega^2-\epsilon)]$ $P/VE_{ext}=[(\epsilon-1)/4\pi V][(q^2/\omega^2-1)/(q^2/\omega^2-\epsilon)]$	$E/E_{ext}=(1-\epsilon)/\epsilon$ $P/VE_{ext}=(\epsilon-1)/4\pi V\epsilon$

[a] cgs units, volume considered is V, wave vector q in units which include the velocity of light.

The contributions of the two types of pole can be separated by defining $\boldsymbol{\kappa}$ as a unit vector parallel to $\mathbf{q}$, and $\boldsymbol{\lambda}$ and $\boldsymbol{\mu}$ as any pair of unit vectors perpendicular to each other and to $\mathbf{q}$. Then using the properties

$$\kappa_1\kappa_2+\lambda_1\lambda_2+\mu_1\mu_2=0 \qquad \kappa_1^2+\lambda_1^2+\mu_1^2=1, \tag{3.26}$$

(3.25) can be written

$$T_{ij}=-\frac{4\pi}{V}\left\{\frac{\kappa_i\kappa_j}{\epsilon}-\frac{\lambda_i\lambda_j+\mu_i\mu_j}{(q/\omega)^2-\epsilon}\right\} \tag{3.27}$$

with the longitudinal and transverse contributions clearly resolved. Table III lists these results for the isotropic case. Equivalent expressions for admittances in the isotropic case have been derived by Abrikosov *et al.* (1963).

The calculations so far in the present subsection refer to the electric-field response to an applied polarization. However the ionic displacement amplitudes $\mathbf{W}^\nu$ are coupled to the electric field $\mathbf{E}$ by the equation of motion (3.1), and the $\mathbf{W}^\nu$ also respond to the applied polarization. The interaction between $\mathbf{W}^\nu$ and $\mathbf{P}^{ext}$ is indirect, and the corresponding response function is a transfer admittance which we define to be

$$T_{ij}{}^\nu=W_i{}^\nu/VP_j{}^{ext}. \tag{3.28}$$

The equation of motion (3.1) can be rewritten more compactly as

$$W_i{}^\nu=\beta^\nu E_i, \tag{3.29}$$

where

$$\beta^\nu=\frac{Z_\nu/M_\nu}{\omega_\nu^2-\omega^2-i\omega\Gamma_\nu}. \tag{3.30}$$

Then, using (3.12), (3.28), and (3.29), we can express the admittance as

$$T_{ij}{}^\nu=\beta^\nu T_{ij}. \tag{3.31}$$

C. The Linear Response to an Applied Mechanical Force

For the fluctuations in $\mathbf{W}^\nu$ we require the ionic-displacement response to an external stimulus. We now remove the externally applied polarization $\mathbf{P}^{ext}$ and instead apply an external force $\mathbf{F}_\nu{}^{ext}$ which tends to distort the crystal in the manner appropriate to normal mode ν. The equation of motion for this mode is thus modified from (3.1) and becomes

$$M_\nu(\omega_\nu^2-\omega^2-i\omega\Gamma_\nu)W_j{}^\nu=Z_\nu E_j+F_{\nu j}{}^{ext}, \tag{3.32}$$

or using (3.29)

$$W_j{}^\nu=\beta^\nu E_j+(\beta^\nu/Z_\nu)F_{\nu j}{}^{ext}. \tag{3.33}$$

All the remaining normal-mode amplitudes continue to satisfy (3.29), and the equation of motion of some randomly chosen normal-mode amplitude $W_i{}^\eta$ can be written in the general form

$$W_i{}^\eta=\beta^\eta E_i+(\beta^\eta/Z_\eta)F_{\nu j}{}^{ext}\delta_{\eta\nu}\delta_{ij}. \tag{3.34}$$

Before deriving an expression for the mechanical response, it is convenient to consider the electric-field response to the applied force. The force term on the right-hand side of (3.33) causes an additional contribution in the ionic polarization evaluated by (3.3), and (3.5) is changed to

$$P_j=[(\epsilon_j-1)/4\pi]E_j+(\beta^\nu/V)F_{\nu j}{}^{ext}. \tag{3.35}$$

But according to (3.9), which is a general result relating $\mathbf{P}$ and $\mathbf{E}$, we have

$$4\pi\omega^2P_j=(q^2-\omega^2)E_j-q_j(\mathbf{q}\cdot\mathbf{E}). \tag{3.36}$$

Elimination of P_j from the last two equations gives

$$(4\pi\omega^2/V)\beta^\nu F_{\nu j}{}^{ext}=(q^2-\epsilon_j\omega^2)E_j-q_j(\mathbf{q}\cdot\mathbf{E}). \tag{3.37}$$

We note that this equation is identical to (3.11) except that $P_j{}^{ext}$ is replaced by $\beta^\nu F_{\nu j}{}^{ext}/V$. It therefore follows that

$$E_i/P_j{}^{ext}=VE_i/\beta^\nu F_{\nu j}{}^{ext}, \tag{3.38}$$

or, using (3.12), (3.28), and (3.31)

$$E_i/F_{\nu j}{}^{ext}=\beta^\nu E_i/VP_j{}^{ext}=\beta^\nu T_{ij}=T_{ij}{}^\nu=W_i{}^\nu/VP_j{}^{ext}. \tag{3.39}$$

The admittance $T_{ij}{}^\nu$ can therefore be defined either as the mechanical response to an external electrical stimulus as in (3.28), or as the electric-field response to an external mechanical stimulus; (3.39) shows that, as would be expected, both definitions lead to the same transfer admittance, proving that the admittance is symmetric. The same result was mentioned for (2.22).

We expect the symmetric form to hold generally for non-magnetic systems.

With these preliminaries we can now calculate the purely mechanical admittances, defined as

$$T_{ij}^{\eta\nu}=W_i^{\eta}/F_{\nu j}^{\text{ext}}. \tag{3.40}$$

Thus, dividing (3.34) by $F_{\nu j}^{\text{ext}}$ and using (3.39), we have

$$T_{ij}^{\eta\nu}=\beta^{\eta}\beta^{\nu}T_{ij}+(\beta^{\eta}/Z_{\eta})\delta_{\eta\nu}\delta_{ij}. \tag{3.41}$$

The two terms in this result are exactly analogous to the two terms in (2.20). For a nonpolar lattice vibration Z_η is zero and β^η vanishes, but the ratio β^η/Z^η remains finite. The transfer admittance is zero for such a vibration and only the second term in the mechanical admittance contributes to give

$$T_{ij}^{\eta\nu}=\delta_{\eta\nu}\delta_{ij}/M_{\eta}(\omega_{\eta}^2-\omega^2-i\omega\Gamma_{\eta}). \tag{3.42}$$

Of somewhat less interest are the response functions for an externally applied electric field. For completeness we list two results for this latter case for the isotropic dielectric in Table III.

D. Fluctuations in Electric Field and Vibrational Amplitude

The response functions obtained in the previous two subsections can be used to derive expressions for the fluctuations in $\mathbf{W}^\nu$ and $\mathbf{E}$. The connection is made via the fluctuation-dissipation or Nyquist theorem discussed in Sec. 1.B. In the present section, we use the theorem to generate some of the standard results for the fluctuations of electric field and lattice displacement.

Consider the simplest possible case of a cubic crystal, where the electric-field response function is given by (3.27). Using (1.1) and (1.3), we have

$$\begin{aligned}\langle E^2(t)\rangle_{\text{Av}}&=\left(\frac{\hbar}{\pi}\right)\int_{-\infty}^{\infty}d\omega[n(\omega)+1]\sum_i \text{Im}\,T_{ii}\\&=-\frac{4\hbar}{V}\int_{-\infty}^{\infty}d\omega[n(\omega)+1]\\&\quad\times\left(\frac{1}{\epsilon}-\frac{2}{(q/\omega)^2-\epsilon}\right).\end{aligned} \tag{3.43}$$

The transverse part of this expression has been given by Case and Chiu (1970).

The frequency spectrum of $\langle E^2(t)\rangle_{\text{Av}}$ can in general only be displayed more transparently by plotting the integrand for specific values of the parameters which enter into the dielectric function. For a cubic crystal having a single resonance at frequency ω_1, from (3.6)

$$\epsilon=\epsilon_\infty+[S_1\omega_1^2/(\omega_1^2-\omega^2-i\omega\Gamma_1)]=\epsilon'+i\epsilon''. \tag{3.44}$$

However, the general result can be further reduced in the limit of zero damping, $\Gamma_1\to 0$ and $\epsilon''\to 0$. For one of the transversely polarized excitations, (3.43) becomes

$$\begin{aligned}\langle E^2(t)_{\text{trans}}\rangle_{\text{Av}}&=\frac{4\pi\hbar}{V}\int_{-\infty}^{\infty}d\omega[n(\omega)+1]\delta\left[\left(\frac{q}{\omega}\right)^2-\epsilon'\right]\\&=\frac{2\pi\hbar}{V}\int_{-\infty}^{\infty}d\omega[n(\omega)+1]\frac{\omega}{\epsilon'^{1/2}}\\&\quad\times[\delta(\omega\epsilon'^{1/2}-q)+\delta(\omega\epsilon'^{1/2}+q)].\end{aligned} \tag{3.45}$$

For a given value of q, the delta-function contributions come in pairs at positive and negative frequency, the contribution for such a $\pm\omega$ pair being

$$\begin{aligned}&\langle E^2(t)_{\text{trans}}\rangle_{\text{Av}}\\&\quad=(2\pi\hbar/V)\{[n(\omega)+1]-[n(-\omega)+1]\}(\omega v_G/\epsilon'^{1/2})\\&\quad=(2\pi\hbar\omega v_G/V\epsilon'^{1/2})[2n(\omega)+1],\end{aligned} \tag{3.46}$$

where (1.20) has been used, and v_G is the usual group velocity of the electromagnetic wave in the dielectric defined as

$$v_G=d\omega/d(\omega\epsilon'^{1/2}). \tag{3.47}$$

For a given q, all the strength of the fluctuation lies at delta-function singularities on the undamped polariton dispersion curve given by (3.24) with the imaginary part of ϵ neglected. A result equivalent to (3.46) can be extracted from Case and Chiu (1970) if only the lowest-order terms in ϵ'' in their Eq. (25) are retained, and some obvious misprints in the succeeding equation are corrected.

A similar treatment of the longitudinal part of (3.43) shows that the fluctuations occur at delta-function singularities of frequency $\pm\omega_L$, the longitudinal mode frequency related to ω_1 by the usual Lyddane–Sachs–Teller relation

$$\omega_L=(\epsilon_0/\epsilon_\infty)^{1/2}\omega_1. \tag{3.48}$$

Here ϵ_0 is the low-frequency dielectric constant

$$\epsilon_0=\epsilon_\infty+S_1. \tag{3.49}$$

The strength of the fluctuations is

$$\begin{aligned}&\langle E^2(t)_{\text{long}}\rangle_{\text{Av}}=(2\pi\hbar\omega_L/V)\\&\quad\times[(\epsilon_0-\epsilon_\infty)/\epsilon_0\epsilon_\infty][2n(\omega_L)+1].\end{aligned} \tag{3.50}$$

Finally we suppose the mode of frequency ω_1 to be nonpolar, so the β^1 defined in (3.30) is zero. This case would be appropriate to describing the long-wavelength optic modes in materials such as diamond, silicon, or germanium. For any of the three polarizations in the limit of zero damping, a calculation based on (3.42) gives delta-function contributions at $\omega=\pm\omega_1$ with strength

$$\langle[W^1(t)]^2\rangle_{\text{Av}}=(\hbar/2M_1\omega_1)[2n(\omega_1)+1]. \tag{3.51}$$

This is the usual expression for the amplitude fluctuations (Peierls, 1955).

E. The Electrooptic Coefficient

We envisage the crystal as being illuminated by a laser beam whose electric field is given by (2.31). The laser beam can mix with the crystal excitations driven by a second electric field of frequency ω to produce sidebands of frequency $\omega_l \pm \omega$. The polarization on the low-frequency side of ω_l, at the frequency ω_s given by (2.34) can be written

$$P_h^s = a_{hij}^{\nu} E_i^l W_j^{\nu *} + b_{hij} E_i^l E_j^*. \tag{3.52}$$

This equation is a generalization of (2.44) for a three-dimensional crystal with several vibrational modes. To avoid many summation signs, we adopt the convention that indices which are repeated in a term (that is ν, i, and j) must be summed. The different coefficients a_{hij}^{ν} and b_{hij} are in general independent and must be determined experimentally for a particular crystal.

Using (3.29) we can write the polarization as

$$P_h^s = [a_{hij}^{\nu} \beta^{\nu *} + b_{hij}] E_i^l E_j^*. \tag{3.53}$$

The quantity in square brackets is a second-order nonlinear susceptibility tensor. The advantage of separating the tensor into two contributions in (3.53) is that a and b are expected to vary smoothly with ω, even as ω passes through lattice resonances [see (2.42) and (2.43)]; the resonant behavior of the nonlinear susceptibility under these conditions appears explicitly in the β^{ν} factors.

The linear electro-optic coefficient r_{hij} is defined in terms of (3.53) for a frequency ω which is much smaller than the lattice resonances ω_{ν} but is sufficiently large not to excite sample acoustic resonances. We neglect ω in (3.30) and obtain

$$\epsilon_h r_{hij} \epsilon_i = -4\pi [a_{hij}^{\nu} (Z_{\nu}/M_{\nu}\omega_{\nu}^2) + b_{hij}], \tag{3.54}$$

where the dielectric functions on the left are to be evaluated at the laser frequency ω_l, and the summation convention does not apply to their subscripts. This result is a generalization of (2.45).

F. Raman Scattering

Let $\mathbf{e}^l$ be the unit polarization vector of the laser beam, and $\mathbf{e}^s$ that of the scattered light. The differential Raman scattering cross section for a unit cell volume V is then obtained by substituting the polarization at the scattered frequency given by (3.52) into (2.57), noting that P in the latter equation must be replaced by $\mathbf{e}^s \cdot \mathbf{P}^s$,

$$d^2\sigma/d\Omega d\omega_s = (n_s V^2 \omega_s^3 \omega_l / n_l c^4) \times \langle | e_h^s e_i^l (a_{hij}^{\nu} W_j^{\nu *} + b_{hij} E_j^*) |^2 \rangle_{\omega_s}, \tag{3.55}$$

where the convention of summing over repeated indices remains in force.

The correlation functions which enter into the thermal average in (3.55) can all be expressed in terms of admittances by means of the fluctuation-dissipation theorem (1.1). We use the definitions (3.12), (3.28) and (3.40), for the various types of response functions, and the relations (3.29) and (3.41) between admittances. The differential cross section can then be written

$$d^2\sigma/d\Omega d\omega_s = (\hbar n_s V^2 \omega_s^3 \omega_l / \pi n_l c^4)[n(\omega)+1] e_h^s e_i^l e_{h'}^s e_{i'}^l \times \mathrm{Im}\{(a_{hij}^{\nu}\beta^{\nu} + b_{hij})(a_{h'i'j'}^{\eta *}\beta^{\eta} + b_{h'i'j'}^*) T_{jj'} + a_{hij}^{\nu} a_{h'i'j'}^{\nu *} (\beta^{\nu}/Z_{\nu})\}, \tag{3.56}$$

where $T_{jj'}$ is given in general by (3.13), (3.14), and (3.15), and β^{ν} is given by (3.30). This result applies generally to a crystal of any symmetry having an arbitrary number of Raman-active vibrational modes. An equivalent expression has been derived by Benson and Mills (1970b).

The general result can be written in more explicit form for the special case of a cubic crystal having a single threefold vibrational mode ω_1. The dielectric constant is given by (3.44), and we note that

$$\beta^1 = \rho(\epsilon - \epsilon_{\infty}) \tag{3.57}$$

where

$$\rho = V/4\pi Z_1. \tag{3.58}$$

Using (3.27) for the response function in the cubic case, we have

$$\frac{d^2\sigma}{d\Omega d\omega_s} = \frac{4\hbar n_s V \omega_s^3 \omega_l}{n_l c^4} [n(\omega)+1] e_h^s e_i^l e_{h'}^s e_{i'}^l \,\mathrm{Im}\left[[a_{hij}^1 \rho(\epsilon-\epsilon_{\infty}) + b_{hij}^1][a_{h'i'j'}^{1*}\rho(\epsilon-\epsilon_{\infty}) + b_{h'i'j'}^{1*}] \times \left(\frac{\lambda_j \lambda_{j'} + \mu_j \mu_{j'}}{(q/\omega)^2 - \epsilon} - \frac{\kappa_j \kappa_{j'}}{\epsilon} \right) + a_{hij}^1 a_{h'i'j'}^{1*} (\lambda_j \lambda_{j'} + \mu_j \mu_{j'} + \kappa_j \kappa_{j'}) \rho^2 (\epsilon - \epsilon_{\infty}) \right], \tag{3.59}$$

where (3.26) has been used in rewriting the final term. If we use the fact that ϵ_{∞} has been assumed purely real, the differential cross section can be written in a form which separates the scattering by transverse and longitudinal excitations. For a transverse excitation of polarization vector $\boldsymbol{\lambda}$, we have

$$\frac{d^2\sigma}{d\Omega d\omega_s} = \frac{4\hbar n_s V \omega_s^3 \omega_l}{n_l c^4} [n(\omega)+1] \,\mathrm{Im}\left(\frac{|a_T|^2 \rho^2 (\epsilon - \epsilon_{\infty})[(q/\omega)^2 - \epsilon_{\infty}] + (a_T b_T^* + a_T^* b_T)\rho(\epsilon - \epsilon_{\infty}) + |b_T|^2}{(q/\omega)^2 - \epsilon} \right), \tag{3.60}$$

where

$$a_T = e_h^s e_i^l \lambda_j a_{hij}^1, \qquad b_T = e_h^s e_i^l \lambda_j b_{hij}. \tag{3.61}$$

This result is to be compared with (2.58) derived for the two-oscillator model. For the longitudinal mode of polarization vector κ, the corresponding result is

$$d^2\sigma/d\Omega d\omega_s = (4\hbar n_s V \omega_s^3 \omega_l / n_l c^4)[n(\omega_L)+1] \times \mathrm{Im}\,[-|\, a_L \rho \epsilon_\infty - b_L\,|^2/\epsilon] \tag{3.62}$$

where

$$a_L = e_h^s e_i^l \kappa_j a_{hij}^1, \qquad b_L = e_h^s e_i^l \kappa_j b_{hij}. \tag{3.63}$$

The somewhat complicated expression (3.60) for the transverse cross section can be simplified by making an approximation which is valid in many cases of practical interest. The denominator in (3.60) is

$$\frac{q^2}{\omega^2} - \epsilon = \frac{(q/\omega)^2 - \epsilon_\infty}{\omega_1^2 - \omega^2 - i\omega\Gamma_1} \times \left(\omega_1^2 - \omega^2 - \frac{S_1\omega_1^2}{(q/\omega)^2 - \epsilon_\infty} - i\omega\Gamma_1\right) \tag{3.64}$$

where (3.44) has been used. The real part of the denominator vanishes at frequencies ω_0 which satisfy

$$q^2/\omega_0^2 = \epsilon_\infty + [S_1\omega_1^2/(\omega_1^2 - \omega_0^2)]. \tag{3.65}$$

Provided that the other factors in the scattering cross section do not vary rapidly with frequency, the maximum in the scattering cross section occurs very near ω_0. Thus, as discussed in Sec. 2 and by Benson and Mills (1970a) the peak in the scattering cross-section occurs close to the dispersion relation for polaritons in the absence of damping.

Provided that the scattering cross section has only a narrow spread about its maximum at ω_0, the frequency ω can be replaced by ω_0 everywhere in the expression for the cross section, except in the term in the real part of the denominator which has a zero at $\omega = \omega_0$. The denominator from (3.64) can thus be written

$$\frac{q^2}{\omega^2} - \epsilon = \frac{2[\epsilon_\infty(\omega_1^2 - \omega_0^2)^2 + S_1\omega_1^4][\omega_0 - \omega - i\Gamma(\omega_0)]}{\omega_0(\omega_1^2 - \omega_0^2)(\omega_1^2 - \omega_0^2 - i\omega_0\Gamma_1)}, \tag{3.66}$$

where (3.65) has been used to remove the dependence on q, and the damping parameter $\Gamma(\omega_0)$ appropriate to a constant q is given by

$$2\Gamma(\omega_0) = \omega_0^2\omega_1^2 S_1\Gamma_1/[\epsilon_\infty(\omega_1^2 - \omega_0^2)^2 + S_1\omega_1^4]. \tag{3.67}$$

The remainder of the scattering cross-section expression (3.60) can be similarly approximated, if we replace ω by ω_0 and use (3.65) to remove q. If we use (3.44) and (3.58), the large bracket of (3.60) becomes,

$$\frac{\omega_0 Z_1^2}{2M_1^2} \cdot \frac{|\, a_T + b_T(M_1/Z_1)(\omega_1^2 - \omega_0^2)\,|^2 - i\,|\, b_T\,|^2\,(M_1/Z_1)^2(\omega_1^2 - \omega_0^2)\omega_0\Gamma_1}{[\epsilon_\infty(\omega_1^2 - \omega_0^2)^2 + S_1\omega_1^4][\omega_0 - \omega - i\Gamma(\omega_0)]}. \tag{3.68}$$

The imaginary term in the numerator is small compared with the real part, except when cancellation occurs between the two terms in the real part. With neglect of the imaginary part, the cross section becomes

$$\frac{d^2\sigma}{d\Omega d\omega_s} = \frac{2\hbar\omega_0 n_s V \omega_s^3 \omega_l Z_1^2}{n_l c^4 M_1^2} \frac{|\, a_T + b_T(M_1/Z_1)(\omega_1^2 - \omega_0^2)\,|^2}{\epsilon_\infty(\omega_1^2 - \omega_0^2)^2 + S_1\omega_1^4} \frac{\Gamma(\omega_0)}{(\omega_0 - \omega)^2 + \Gamma(\omega_0)^2}[n(\omega_0)+1]. \tag{3.69}$$

The cross-section is thus predicted to have a Lorentzian lineshape of width $2\Gamma(\omega_0)$ given by (3.67). The width will be discussed further in Sec. 4.C. Integration of (3.69) over ω_s, remembering that $\omega = \omega_l - \omega_s$, replaces the Lorentzian factor by π to give an expression for $d\sigma/d\Omega$ identical to earlier results derived from a different point of view (Loudon, 1969).

For 90° light scattering, where

$$q/\omega \gg \epsilon^{1/2}, \tag{3.70}$$

the transverse polariton frequency ω_0 approaches ω_1 and the cross section given by (3.60) or (3.69) becomes

$$\frac{d^2\sigma}{d\Omega d\omega_s} = \left(\frac{\hbar n_s V^2 \omega_s^3 \omega_l\,|\, a_T\,|^2\,[n(\omega_1)+1]}{2\pi n_l c^4 M_1 \omega_1}\right)\left(\frac{(\Gamma_1/2)}{(\omega_1 - \omega)^2 + (\Gamma_1/2)^2}\right). \tag{3.71}$$

The linewidth is Γ_1 as expected for a mode which is now entirely mechanical. The longitudinal mode has a cross section given by (3.62), which can be written more explicitly using (3.44) as

$$\frac{d^2\sigma}{d\Omega d\omega_s} = \left(\frac{\hbar n_s V^2 \omega_s^3 \omega_l\,|\, a_L - b_L(4\pi Z_1/\epsilon_\infty V)\,|^2\,[n(\omega_L)+1]}{2\pi n_l c^4 M_1 \omega_L}\right)\left(\frac{(\Gamma_1/2)}{(\omega_L - \omega)^2 + (\Gamma_1/2)^2}\right). \tag{3.72}$$

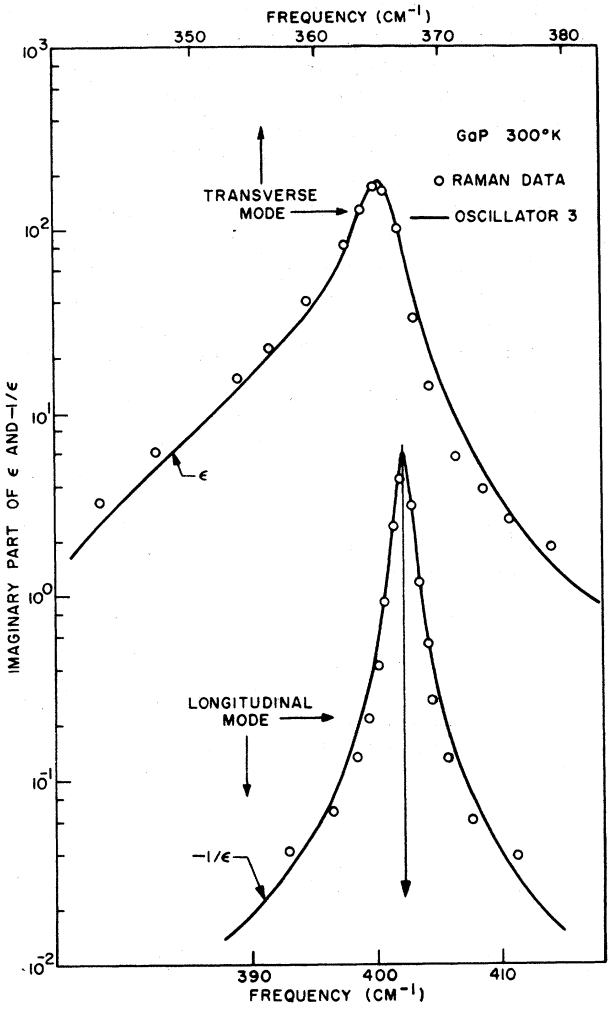

FIG. 8. Transverse and longitudinal optic mode scattering in GaP. The measured Raman intensities have been scaled to fit the dielectric functions near the peaks. The solid curve corresponds to a dielectric function which includes frequency dependent damping due to a two-phonon band near 357 cm^{-1} (Barker, 1968).

The longitudinal mode also has linewidth Γ_1. Most previous calculations have derived $d\sigma/d\Omega$, where the Lorentzian factors in (3.71) and (3.72) are replaced by π. Results equivalent to the above have been obtained in a wide variety of notations by previous authors.

All the results subsequent to (3.56) refer to a cubic crystal having a single vibrational mode which would be threefold degenerate for $Z_1=0$. The particular simplification which occurs in this case is due to the way in which β^1 is related to the dielectric function by (3.57). For crystals having several degrees of freedom or optical anisotropy, the cross section must be evaluated using (3.56). The qualitative behavior of the cross section as a function of frequency is especially simple for the cubic-crystal single-vibration case, and will be further discussed in Sec. 4.

4. APPLICATIONS

A. Right-Angle Scattering

The case of right-angle scattering, briefly mentioned at the end of the previous section, is applicable to the great majority of experiments. If a crystal has a transverse lattice resonance at ω_1, and ϵ asymptotically approaches ϵ_0 below the resonance, then the region

$$q \gg \omega_1 \epsilon_0^{1/2} \tag{4.1}$$

lies well to the right of the region of mixed mode behavior. In this large-q region, the polariton dispersion curve near ω_1 is horizontal. For most crystals, scattering at 90° selects q in this regime. For a cubic crystal we can take the cross section derived in Sec. 2.G, and take the large-q limit directly to obtain

$$(d^2\sigma/d\Omega d\omega_s)_{\text{trans}} = A[n(\omega)+1]\,\text{Im}\,(\epsilon) \tag{4.2}$$

for transverse lattice waves, and

$$(d^2\sigma/d\Omega d\omega_s)_{\text{long}} = A[n(\omega)+1] \times \text{Im}\,\{[\epsilon_\infty+(Z/z)(\epsilon_\infty-1)]^2/-\epsilon\} \tag{4.3}$$

for longitudinal lattice waves. A is a constant to a good approximation under nonresonant conditions. It contains the nonlinear parameter α and the various indices of refraction and resonant denominators which appear in (2.58). Similar expressions for scattering cross sections are obtained from the results of Sec. 3.F.

It is seen from (4.2) and (4.3) that for 90° scattering the Raman spectra are given essentially by $[n(\omega)+1]\,\text{Im}\,(\epsilon)$ and $[n(\omega)+1]\,\text{Im}\,(-1/\epsilon)$. These forms have been used in a study of scattering in GaP where the dielectric function is so peaked that even the frequency dependence of the thermal factor could be neglected (Barker, 1968). Figure 8 shows the scattering spectra.

DiDomenico *et al.* (1968) have studied 90° scattering in $BaTiO_3$. For the frequencies observed in this experi-

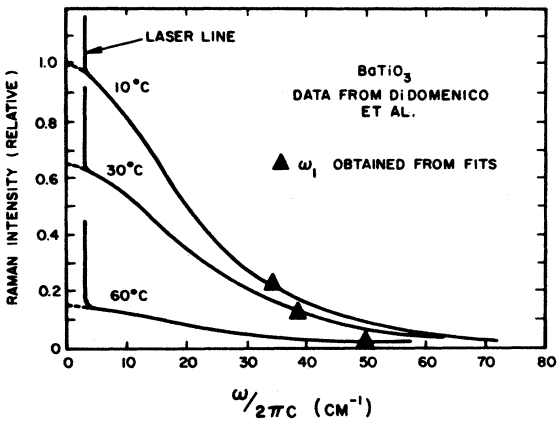

FIG. 9. Raman spectrum of $BaTiO_3$ in the ferroelectric phase. The sample is being cooled towards the second phase transition near 0°C. Analyses of these spectra give the mode frequencies shown by solid triangles.

ment $k_BT \gg \hbar\omega$, and the thermal factors become $k_BT/\hbar\omega$. The spectral peaks are so broad that the frequency dependence contained in the thermal factor k_BT/ω is extremely important. Their Raman spectra are shown in Fig. 9. While Im (ϵ) has a peak, it is so broad that it disappears in the function Im (ϵ/ω) of (4.2) taken in the classical limit. DiDomenico *et al.* use (4.2) to analyze for the transverse mechanical resonant frequency ω_1 shown as triangles in Fig. 9.

Kaminow and Damen (1968) have analyzed the Raman scattering from paraelectric KH_2PO_4. In this case the spectra extend to high frequencies so that $k_BT \gg \hbar\omega$ is not a good approximation. Figure 10(a) shows the spectra of Kaminow and Damen. Both Stokes and anti-Stokes spectra were measured. In Fig. 10(b), the spectra have been corrected for the quantum prefactor to yield a quantity proportional to Im (ϵ). Here, as in $BaTiO_3$, the peak in Im (ϵ) is so broad that the scattering spectrum shows no peak. The use of (4.2) is therefore essential in analyzing for the shape of ϵ and the resonant frequency and damping parameters it contains.

Scattering by longitudinal modes has not been observed in the studies of $BaTiO_3$ and KH_2PO_4 discussed above. Barker (1970) has analyzed the case of an oscillator with very large damping and shown that

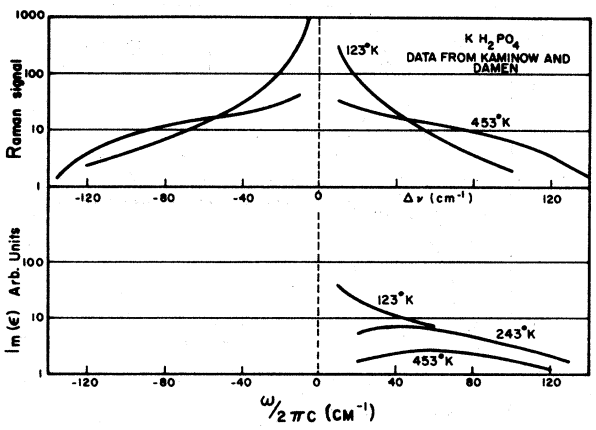

FIG. 10. The Raman spectra of KH_2PO_4 above the transition temperature. The lower figure shows the signal corrected for the quantum thermal factor to give the dielectric response function which is very broad.

the longitudinal spectrum can be expected to be quite featureless similar to the transverse spectra discussed above. Some general comments can be made about the strength of the longitudinal scattering using (4.2) and (4.3). Taking the ratio of the integrated strengths for a one-oscillator dielectric model, we find

$$\frac{(d\sigma/d\Omega)_{\text{trans}}}{(d\sigma/d\Omega)_{\text{long}}} = \int_{-\infty}^{\infty} \text{Im}\,(\epsilon)\omega^{-1}\,d\omega \Big/ \left([\epsilon_\infty + (Z/z)(\epsilon_\infty - 1)]^2 \int_{-\infty}^{\infty} \text{Im}\,(-1/\epsilon)\omega^{-1}\,d\omega \right), \tag{4.4}$$

where we have used the equivalence of integration over ω and ω_s for fixed ω_l, and have included the classical form of the thermal factor in (4.2) and (4.3). This is a good approximation if Im (ϵ) and Im ($-1/\epsilon$) fall off rapidly, at and above the frequency $k_BT/\hbar$. The integrals in (4.4) can be evaluated exactly for a classical oscillator (2.12) giving:

$$\frac{(d\sigma/d\Omega)_{\text{trans}}}{(d\sigma/d\Omega)_{\text{long}}} = \frac{\epsilon_0\epsilon_\infty}{\{[\epsilon_\infty + (Z/z)(\epsilon_\infty - 1)]^2\}}. \tag{4.5}$$

Equation (4.5) shows that the ratio of integrated strengths of the transverse to longitudinal modes is determined by only the high- and low-frequency dielectric constants and the ratio of the charges in the two-oscillator model of Sec. 2. In GaP, $\epsilon_0 = 11.1$ and $\epsilon_\infty = 9.09$ (Barker, 1968). The cancellation shown in Fig. 6 which was predicted by Faust and Henry (1966) determines Z/z to be 0.5. Using these numbers, (4.5) predicts that the transverse mode is weaker than the longitudinal, the intensity ratio being 1:1.7. This is the ratio observed by Faust and Henry (1966) (see also Faust *et al.*, 1968).

On the basis of the magnitudes of ϵ_0, ϵ_∞, and estimates of the electronic parameters in a variety of crystals, we expect Z/z never to depart very far from unity. In paraelectric and ferroelectric crystals therefore where $\epsilon_0 \gg \epsilon_\infty$, 90° scattering should show the transverse modes much stronger than the corresponding longitudinal modes according to (4.5). This behavior is observed in $LiNbO_3$ (Barker and Loudon, 1967; Kaminow and Johnston, 1967). The same effect may be responsible for the difficulty in observing the longitudinal mode in KH_2PO_4 (Kaminow, 1969) and in $NH_4H_2PO_4$, both of which have large ratios of $\epsilon_0/\epsilon_\infty$.

The oscillator model of Sec. 2 was used to derive the simple relations (4.2) and (4.3) between the dielectric functions and Raman cross section. These relations can be shown to hold even when $\epsilon(\omega)$ contains complicated frequency dependent damping and for certain cases in which there is more than one-phonon oscillator. Stolen (1970) has found (4.2) to hold in the case of noncrystalline glasses where Im (ϵ) is thought to arise from a broad distribution of modes. The reader is cautioned however that there can be more complicated situations where (4.2) and (4.3) do not hold. Scott *et al.* (1970) have discussed such a case for scattering by plasmons and phonons in doped CdS, where there is a pronounced interference in the scattering by the two types of excitations. Such effects can be included in the oscillator model only at the expense of simplicity by including two or more ionic vibrators which are coupled.

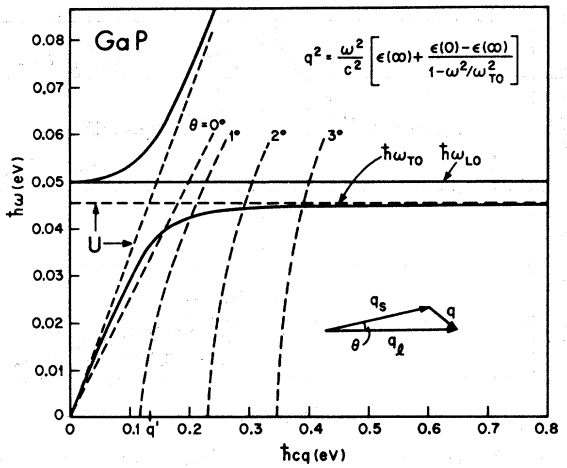

FIG. 11. Polaritons in gallium phosphide. The dispersion curves of the uncoupled phonons and photons are shown by the lines labeled U, and those of the LO phonons and the polaritons by solid lines. The equation of the polariton lines is indicated. The long-dashed curves indicate the values of energy and wave vector which kinematically are possible at each angle θ, where θ is defined by the vector triangle. q_l and q_s are the wave vectors of the laser light and the Stokes shifted light, respectively; q is the wave vector of the scattered polariton. (From Henry and Hopfield, 1965).

B. Experiments on Polariton Light Scattering

In Sec. 4.A, the large-q Raman scattering regime was discussed. In that regime the lower polariton dispersion curve is flat and the mode consists principally of mechanical vibration. We now examine the small-q region where the polariton has a significant dispersion, i.e., there is a significant admixture of electric field and mechanical ion displacement in the mode. In previous theoretical plots (Figs. 5 and 6) contours of modes at constant q were plotted giving the impression that q is an independent variable. For the experimenter this is not so at the present time. The conservation of wave vector gives

$$\mathbf{q}=\mathbf{q}_l-\mathbf{q}_s. \tag{4.6}$$

In all present Raman setups, the lens which directs the laser light into the crystal and the lens which selects the scattered light are fixed with respect to the crystal. Since $q_s=n_s\omega_s/c$, where n_s is the index at the scattered frequency, when different frequencies ω_s are studied by scanning with a spectrometer, q_s is changed also, changing q. The effect of scanning ω_s is to trace out a contour in (q, ω) space which depends on n_s and its dispersion.

Henry and Hopfield (1965) have discussed the situation for GaP with 6328 Å He–Ne laser excitation. Figure 11 is taken from their paper. The insert in Fig. 11 shows the wave-vector conservation vector triangle. The angle θ is measured in the medium. Using accurate values of n_l and n_s appropriate to the He–Ne laser, frequency scans of ω at constant θ give the contours shown in Fig. 11. Two points are immediately apparent. First we note that the experimental scans cross the dispersion curve at an angle. This effect can cause asymmetric line shape and an observed linewidth somewhat different from that calculated for constant-q spectra. Secondly, certain portions of the lower and upper polariton curve may be inaccessible because of reaching a limiting q value at $\theta=0°$. In GaP (with 6328 Å excitation), the lower branch can be studied down to about 304 cm^{-1}. Figure 12 shows the experimental results of Henry and Hopfield (1965) for GaP. The experimental peaks in the scattering give a pleasing confirmation of the polariton dispersion curve.

Loudon (1963a, 1964) has discussed the polariton curves and features of the Raman scattering to be expected for uniaxial crystals. The dispersion curves are obtained as discussed in Sec. 3, Eqs. (3.19) and (3.20). The scattering intensity is given by (3.56). Figure 13 shows the results of polariton scattering experiments in the uniaxial crystal ZnO carried out by Porto *et al.* (1966). The polaritons polarized along y have been measured for two different polarizations of the laser. On the left of the figure, the laser is polarized perpendicular to z (ordinary ray) which in ZnO allows measurements to be made down to lower polariton frequencies. The measurements show good agreement with the polariton dispersion curve.

Polariton scattering measurements have been carried out in ZnSe by Leite, Damen, and Scott (1969). These authors make some comparisons with the predicted scattering intensity as well as the mode frequency. Scott, Cheesman, and Porto (1967), and Scott and Ushioda (1969) have measured polariton scattering in α-quartz which possesses eight polariton

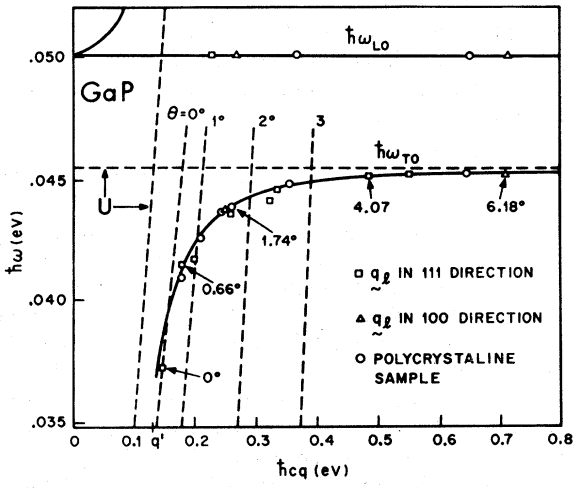

FIG. 12. A plot of the observed energies and wave vectors of the polaritons and of the LO phonons; the theoretical dispersion curves for the uncoupled photons and phonons are shown by lines labeled U. The values of energies and wave vectors which are kinematically possible at angle θ are shown by dashed lines. Some of the experimental angles θ are indicated next to the data points (Henry and Hopfield, 1965).

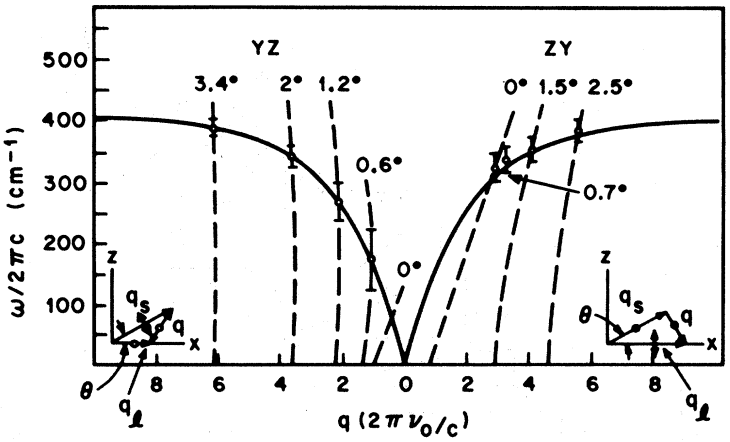

FIG. 13. The dispersion curves for polaritons in ZnO. The theoretical dispersion curves are shown by solid lines, and the allowed $\omega(q)$ curves for different $\theta(\omega_l=6328$ Å) are shown by dashed lines. The experimental points are the energies and wave vectors of the polaritons derived from small angle scattering measurements, and the vertical bars represent the line width at half-maximum, of the observed Raman peaks. The inserts represent the "kinematics" for the two configurations $X(YZ)X$ and $X(ZY)X$. The single arrows and dots indicate polarization in and normal to the plane of propagation q_l, q_s, and q and are the wave vectors of the incident laser radiation, Stokes scattered radiation ($\omega_s=\omega_l-\omega_q$), and polaritons, respectively. (From Porto, Tell, and Damen 1966).

branches. Using what is essentially the eight mode form of (3.56), Scott and Ushioda present plots of the polariton intensities and comment on the stimulated Raman gain to be expected for the strong 128 cm^{-1} resonance. Detailed theory of polariton scattering and some comparisons with experiment have been given in a series of articles by Burstein (1969) and Burstein and Mills (1969a, b).

Figure 14 shows polariton scattering from the A_1 symmetry 628 cm^{-1} mode in $LiNbO_3$ (Puthoff *et al.*, 1968). The authors plot for comparison (dashed curve) the real part of q by using the expression

$$q=\omega(\epsilon')^{1/2}/c. \tag{4.7}$$

While this procedure has some relevance in discussing driven infrared response, it is inappropriate for Raman scattering. From Fig. 14 we note that this procedure gives a maximum q. As is apparent in studying the equations in Sec. 2.C, there is no limit on the q of a driving field used to define a response function, and

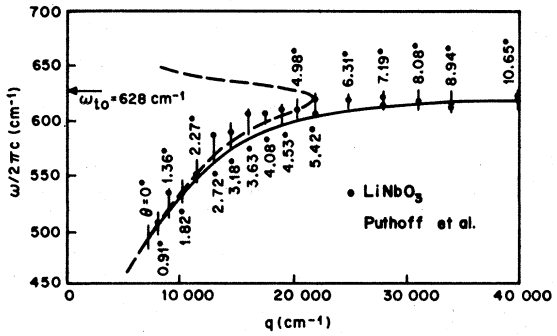

FIG. 14. Comparison of theory and experiment in $LiNbO_3$ (from Puthoff *et al.* 1957). The short nearly vertical lines are frequency–wave vector conservation curves and are labeled by the angular separation θ between Stokes and laser beams. The dashed curve is drawn by the authors from infrared data. The solid curve is the polariton dispersion curve [Eq. (2.27)]. It fits the points in a reasonable way particularly at large q as discussed in the text.

hence no limit on the q transferred to the lattice in Raman scattering. Since several authors have used (4.7) to define the polariton dispersion curve (see most recently Zallen *et al.*, 1970), it is worth emphasizing its real significance. If a dielectric is driven at one plane by a field $E\exp(-i\omega t)$, then a plane wave is set up in the medium which has an exponentially decaying characteristic. By solving Maxwell's equations with no sources in the dielectric, (4.7) is obtained for the real part of the wave vector of the wave. This situation corresponds to an infrared beam incident on the surface of a dielectric but has little connection with the homogeneous volume drive associated with a laser beam entering a transparent medium. In Fig. 14 we have plotted as a solid curve the polariton dispersion in $LiNbO_3$ using (2.27). This curve fits the data reasonably well at low q and is much more satisfactory at large q. Recently, Klyshko *et al.* (1970) have discussed polariton scattering in $LiNbO_3$ for frequencies above all lattice modes, i.e., for the highest frequency polariton branch. They find a cancellation in cross-section in the small-θ region.

Pinczuk *et al.* (1969) have observed Raman scattering by polaritons in tetragonal $BaTiO_3$. Their results have been analyzed theoretically by Benson and Mills (1970b) using a theory similar to that outlined in Sec. 3. Two polariton modes are observed, and the theory must take account of interference effects. Full account must also be taken of the actual crossing of the constant-θ scans with the polariton dispersion curve. Benson and Mills achieve excellent agreement with the observed lineshapes for a range of angles θ. The same authors (1970a) have calculated the experimental linewidth to be expected in cubic ZnSe.

Obukhovskii *et al.* (1970) have given a theory of light scattering by polaritons which is similar in some respects to that of Sec. 3. They relate their theory to the particular examples of CdS and $LiNbO_3$ and obtain agreement with the measurements of Klyshko *et al.* mentioned above.

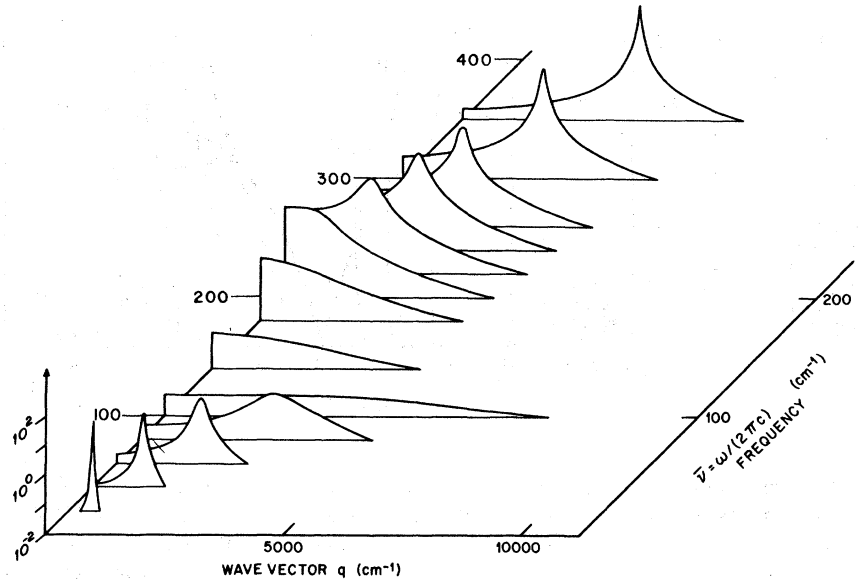

FIG. 15. Polariton response function. This is the same function shown in Fig. 5(a) but drawn for constant frequency contours.

C. Sum Rules and Linewidths

In this section we study the form of the polariton response function $T=[(q/\omega)^2-\epsilon]^{-1}$. We restrict discussion to cubic crystals and in some places to one mechanical resonance. The generalization to more complicated situations is straightforward. Several results concerning the linewidth of the peak of Im (T) in ω space and in q space as well as the strength of the peak can be derived. These results have some interest and application though it is well to recall that the actual Raman scattering spectrum may deviate from these results. The deviations occur because of the multiplying factor which is included with T in determining the scattering. The deviations can be exceedingly large near a cancellation such as occurs near 260 cm^{-1} in GaP (Fig. 6).

One of the Kramers–Kronig relations (Kittel, 1958, 1969) may be applied directly to the response function T to give:

$$\frac{2}{\pi}\int_0^\infty \mathrm{Im}\,\{(q/\omega)^2-\epsilon\}^{-1}\frac{d\omega}{\omega}=\epsilon_\infty^{-1}. \qquad (4.8)$$

This result is independent of q. Equation (4.8) shows that the weighted area under the polariton peaks is constant. In the case where there is one transverse mechanical resonance as shown in Fig. 5, there are two peaks for any value of q. At large q, the lower peak gets very weak (see Fig. 5). Equation (4.8) shows that the upper peak, when weighted by the $1/\omega$ factor in the integral, must have an area which approaches $\pi/(2\epsilon_\infty)$.

We next examine the width of the polariton peaks along contours of constant ω. Figure 15 shows the polariton response function of Fig. 5 replotted in this way. The response function may be written

$$-\omega^2/[\omega^2\,\mathrm{Re}\,(\epsilon)-q^2+i\omega^2\,\mathrm{Im}\,(\epsilon)]. \qquad (4.9)$$

Equation (4.9) shows that for constant ω, the response as a function of q has Lorentzian form. If Im (ϵ) is not too large, the peak has a width at half-maximum of:

$$\delta q \approx \omega\,\mathrm{Im}\,(\epsilon)/[\mathrm{Re}\,(\epsilon)]^{1/2}\approx 4\pi k/\lambda, \qquad (4.10)$$

where k is the optical extinction coefficient, and λ the wavelength in free space of a wave with frequency ω. Here $4\pi k/\lambda$ will be recognized as the attenuation coefficient, usually denoted α, so that the final result may be compactly written as:

$$\delta q \approx \alpha. \qquad (4.11)$$

The approximation used to obtain (4.11) is essentially that Re $(\epsilon)\gg$Im (ϵ). This condition is usually met as long as the constant ω contour we wish to study is well away from the mechanical resonances at ω_1 and ω_L. Figure 15 shows that near these frequencies the constant ω contours become very asymmetric and broad. Coffinet and De Martini (1969) first pointed out the utility of (4.11). These authors devised an experimental arrangement using essentially two different laser frequencies to generate a polariton parametrically, then a third beam to detect the polariton by scattering from it. By varying the angle between two of the beams, a scan

of q at constant ω was made. Using (4.11) the infrared attenuation can be measured entirely by optical laser probes. The authors make a study of the infrared attenuation in GaP and note that this method can measure even very large values of α deep within a crystal. The technique of constant ω scans appears to be a new and useful technique for study of dispersion curves.

An expression for the width of the polariton peak along a contour of constant q has already been given in (3.67). Note that $2\Gamma(\omega_0)$ reduces to $2\Gamma_1$, both at the transverse frequency ω_1 and at the longitudinal frequency $\omega_L=(\epsilon_0/\epsilon_\infty)^{1/2}\omega_1$. The linewidth expression cannot be used in between these frequencies, since (3.65) has no real solutions, but it applies for all other ω_0. The linewidth $2\Gamma(\omega_0)$ can be regarded as an expression of the finite lifetime of the polariton in the presence of lattice damping. An expression for the polariton relaxation rate in the small damping limit has been given in Eq. (32) of Loudon (1970). With suitable changes in notation ($A^2\rightarrow S_1\omega_1^2/\epsilon_\infty$, $\Gamma\rightarrow\Gamma_1$, $\omega_0\rightarrow\omega_1$, $\omega\rightarrow\omega_0$) this equation is exactly the same as (3.67).

Finally we derive some relations for the peaks in the response function at constant-q when ϵ is given by a single damped-oscillator form. We take

$$\epsilon=\epsilon_\infty+[S\omega_1^2/(\omega_1^2-\omega^2-i\omega\Gamma_1)]$$
$$=\epsilon_\infty(\omega_L^2-\omega^2-i\omega\Gamma_1)/(\omega_1^2-\omega^2-i\omega\Gamma_1), \quad (4.12)$$

where we have used the Lyddane–Sachs–Teller relation for a damped oscillator (Barker, 1964) to introduce the longitudinal mode frequency ω_L. If we multiply top and bottom by certain factors, the polariton response function (2.27) becomes

$$\frac{(\omega_1^2-\omega^2-i\omega\Gamma_1)\omega^2/\epsilon_\infty}{D}, \quad (4.13)$$

where the denominator is

$$D=\omega^4+i\Gamma_1\omega^3-[\omega_L^2+(q^2/\epsilon_\infty)]\omega^2$$
$$-i\Gamma_1\omega(q^2/\epsilon_\infty)+\omega_1^2(q^2/\epsilon_\infty). \quad (4.14)$$

The zeros of D determine the poles of the polariton response function: if ω is a root of D, so is $-\omega^*$. Thus the poles of the response function occur in pairs. The two members of a pair are mirror images—mirrored in the imaginary frequency axis. Because of the occurrence of pairs of poles, it is convenient to factor D into quadratic rather than linear factors. We choose the form

$$D=(\omega_a^2-\omega^2-i\omega\Gamma_a)(\omega_b^2-\omega^2-i\omega\Gamma_b). \quad (4.15)$$

The form (4.15) explicitly shows the two different pole pairs that occur in the response function (i.e., the two branches of the polariton dispersion curve). The peaks are near ω_a and ω_b and have linewidths determined by Γ_a and Γ_b. It is interesting to now relate these two peaks to the parameters ω_1, ω_L, and Γ_1 which define ϵ in (4.12). Comparing coefficients in (4.14) and (4.15) we obtain the four results

$$\Gamma_a+\Gamma_b=\Gamma_1, \quad (4.16)$$

$$\omega_a^2+\omega_b^2+\Gamma_a\Gamma_b=\omega_L^2+(q^2/\epsilon_\infty), \quad (4.17)$$

$$\Gamma_a\omega_b^2+\Gamma_b\omega_a^2=\Gamma_1(q^2/\epsilon_\infty), \quad (4.18)$$

$$\omega_a^2\omega_b^2=\omega_1^2(q^2/\epsilon_\infty). \quad (4.19)$$

Equation (4.16) shows that independent of q the sum of the damping factors for the two polariton peaks is equal to the damping factor entering ϵ. This effect can be seen in Fig. 5. As q increases, the width of the lower branch increases but there is a concomitant decrease in the linewidth of the upper polariton branch.

Several other results may be obtained from the above equations. We will note only two. As q approaches zero, one polariton peak must approach zero linearly with q and its damping factor approaches zero as q^2. Secondly, (4.19) may be considered the analog of the Lyddane–Sachs–Teller relation, giving a useful relation between the product of the mode frequencies[9] at any q. Combined with the other relations, (4.19) shows that at large q the upper polariton peak frequency increases linearly with q and has phase velocity $c/(\epsilon_\infty)^{1/2}$ as expected for a light wave in the medium.

D. Polaritons in Orthorhombic Crystals

The polariton dispersion relations derived in Sec. 3.B for uniaxial and cubic crystals have all been obtained previously and have been discussed in the literature. However the orthorhombic crystal dispersion relations obtained by substituting (3.15) in (3.16) have not been previously published,[10] and we discuss here the main features of polaritons in such crystals.

For any direction of propagation $\mathbf{q}$ in an orthorhombic crystal (possible point groups D_2, C_{2v}, and D_{2h}), the polariton branches are nondegenerate. Except when $\mathbf{q}$ lies in a plane containing two of the principal axes, the polaritons do not possess simple pure transverse or pure longitudinal polarization. If the three components ϵ_1, ϵ_2, and ϵ_3 of the dielectric function have a total of n resonances, then (3.16) is of order $n+2$ in ω^2, and $n+2$ distinct polariton branches occur for each wave vector q.

---

[9] By mode frequencies we mean the real numbers ω_a or ω_b which will be recognized as the distance from the origin to the pole of the response function.

[10] *Note added in proof:* These dispersion relations have in fact been derived previously by L. Merten in a reference which we overlooked (Phys. Stat. Solidi, **30**, 449, 1968).

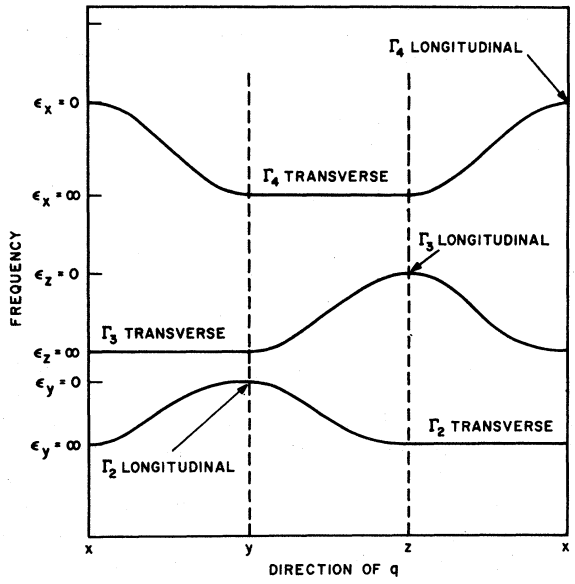

FIG. 16. Schematic diagram of the variations of the frequencies of large q excitations with wave-vector direction in the principal planes of an orthorhombic crystal. The excitations have mixed polarization except where labeled transverse or longitudinal. The pure longitudinal excitations occur only at isolated points along the dispersion curves. Two additional branches occur at much higher frequency and correspond to ordinary and extraordinary light waves.

This rule is consistent with the well-known result for cubic crystals having a single threefold degenerate pole, where for each $\mathbf{q}$ there are five solutions of (3.16), except that twofold degeneracies remain for the cubic case.

The polariton dispersion relation (3.16) factorizes when $\mathbf{q}$ lies in a principal plane. Suppose that $\mathbf{q}$ lies in the plane which contains principal axes 1 and 2. With q_3 set equal to zero, (3.15) combined with (3.16) factors into two equations

$$q_1^2+q_2^2=\epsilon_3\omega^2, \tag{4.20}$$

$$\epsilon_1 q_1^2+\epsilon_2 q_2^2=\epsilon_1\epsilon_2\omega^2. \tag{4.21}$$

The first type of solution is similar to the result (3.24) for a cubic crystal. The polaritons corresponding to this solution are transversely polarized for any direction of $\mathbf{q}$ in the $q_3=0$ plane; the polariton frequencies are independent of the direction of $\mathbf{q}$. The second type of solution (4.21) is similar to (3.20) for a uniaxial crystal; the polaritons are in general of mixed polarization but become strictly transverse or longitudinal for both $q_1=0$ and $q_2=0$. The frequencies of the polaritons resulting from (4.21) vary with the direction of $\mathbf{q}$ in the $q_3=0$ plane.

For right angle light scattering, where excitations having $q\gg\omega$ are observed, the mode frequencies are obtained by retaining only the terms in (3.15) of highest order in $\mathbf{q}$. Krauzman (1970) has recently considered this case. The equation to be solved is

$$\epsilon_1 q_1^2+\epsilon_2 q_2^2+\epsilon_3 q_3^2=0. \tag{4.22}$$

The type of solution is illustrated in Fig. 16 which shows the excitation frequencies as functions of q direction for a fixed $|\mathbf{q}|$ for the three principal planes of an orthorhombic crystal. The crystal is a hypothetical substance of D_2 symmetry having one resonance in each of the dielectric functions ϵ_x, ϵ_y, and ϵ_z. The symmetries of vibrations parallel to x, y, and z, are Γ_4, Γ_2, and Γ_3, respectively in the notation of Koster *et al.* (1963). The excitations in Fig. 16 are of mixed symmetry and polarization except where the curves are labeled with an irreducible representation and a polarization. These parts of the curves correspond to infinities or zeros in components of the dielectric function as indicated in the figure. Note that the excitations can be transverse over an entire principal plane, but that longitudinal excitations can occur only when $\mathbf{q}$ points parallel to a principal axis. The other two solutions of (3.15) and (3.16) for the value of $|\mathbf{q}|$ assumed in Fig. 16 occur at much higher frequencies and have ω and $|\mathbf{q}|$ of the same order of magnitude. These modes correspond to the two types of light wave which can be propagated in an orthorhombic crystal.

Curves of the type shown in Fig. 16 could be measured experimentally by right angle Raman scattering. Except where the excitations are longitudinal they also cause infrared absorption, and the variation of frequency with wave vector direction could be determined by analysis of a series of absorption or reflection measurements on suitably oriented samples. Couture *et al.* (1970) have recently carried out experimental and theoretical light scattering studies of this type on crystals of orthorhombic iodic acid HIO_3. Hartwig *et al.* (1971) have studied orthorhombic $NaNO_2$ and have derived the large wave-vector formula (4.22). For $NaNO_2$, the angular dispersion curves equivalent to Fig. 16 have eight branches. The authors have measured five branches in one symmetry plane and discussed the angular dispersion and intensity.

E. Resonance Effects

In the two-oscillator model of Sec. 2, the electro-optic effect and the light-scattering cross section were expressed in terms of two coefficients, a and b. Explicit expressions for a and b in terms of the parameters of the model are given in Eqs. (2.42) and (2.43). The coefficients show resonance behavior when ω_l or ω_s approach the electronic frequency $(k/m)^{1/2}$. In the present subsection we exhibit the analogous quantum-mechanical expressions for a and b, and discuss the resonant behavior of the cross section.

The quantum-mechanical generalizations of a and b, namely $a_{hij}{}^{\nu}$ and b_{hij}, have been introduced in (3.52). A quantum-mechanical treatment of light scattering by pure lattice vibrations has been given by Loudon (1963b). The quantum-mechanical expression for $a_{hij}{}^{\nu}$ can be found by comparing Eq. (22) of this last reference with (3.71) of the present paper. In making the comparison the two equations must be modified slightly to represent the cross section $d\sigma/d\Omega$ and various changes of notation must be taken into account. The resulting expression is

$$a_{hij}{}^{\nu}=\frac{e^2}{\hbar^2 dV}\sum_{\alpha,\beta}\left\{\frac{r_{0\beta}{}^{h}r_{\beta\alpha}{}^{i}\Xi_{\alpha 0}{}^{\nu j}}{(\omega_\beta-\omega_s)(\omega_\alpha+\omega)}+\frac{r_{0\beta}{}^{i}r_{\beta\alpha}{}^{h}\Xi_{\alpha 0}{}^{\nu j}}{(\omega_\beta+\omega_l)(\omega_\alpha+\omega)}\right.$$
$$+\frac{r_{0\beta}{}^{h}\Xi_{\beta\alpha}{}^{\nu i}r_{\alpha 0}{}^{i}}{(\omega_\beta-\omega_s)(\omega_\alpha-\omega_l)}+\frac{r_{0\beta}{}^{i}\Xi_{\beta\alpha}{}^{\nu i}r_{\alpha 0}{}^{h}}{(\omega_\beta+\omega_l)(\omega_\alpha+\omega_s)}$$
$$\left.+\frac{\Xi_{0\beta}{}^{\nu i}r_{\beta\alpha}{}^{h}r_{\alpha 0}{}^{i}}{(\omega_\beta-\omega)(\omega_\alpha-\omega_l)}+\frac{\Xi_{0\beta}{}^{\nu i}r_{\beta\alpha}{}^{i}r_{\alpha 0}{}^{h}}{(\omega_\beta-\omega)(\omega_\alpha+\omega_s)}\right\},\quad(4.23)$$

where α and β refer to electron–hole pair states of excitation energies ω_α and ω_β, 0 refers to the electronic ground state, d is the lattice constant, $\Xi_{\alpha\beta}{}^{\nu j}$ is the deformation potential matrix element for the vibrational mode $W_j{}^{\nu}$ between the pair states α and β, and the electron momentum matrix elements used in the above reference have been converted to r matrix elements.

In a similar way, the quantum-mechanical expression for b_{hij} can be obtained from the equations of Sec. 5 of Loudon (1963b). With the same notation and modifications used in writing (4.23) above, we find

$$b_{hij}=\frac{e^3}{\hbar^2 V}\sum_{\alpha\neq\beta}\left\{\frac{r_{0\beta}{}^{h}r_{\beta\alpha}{}^{i}r_{\alpha 0}{}^{j}}{(\omega_\beta-\omega_s)(\omega_\alpha+\omega)}+\frac{r_{0\beta}{}^{i}r_{\beta\alpha}{}^{h}r_{\alpha 0}{}^{j}}{(\omega_\beta+\omega_l)(\omega_\alpha+\omega)}\right.$$
$$+\frac{r_{0\beta}{}^{h}r_{\beta\alpha}{}^{j}r_{\alpha 0}{}^{i}}{(\omega_\beta-\omega_s)(\omega_\alpha-\omega_l)}+\frac{r_{0\beta}{}^{j}r_{\beta\alpha}{}^{i}r_{\alpha 0}{}^{h}}{(\omega_\beta+\omega_l)(\omega_\alpha+\omega_s)}$$
$$\left.+\frac{r_{0\beta}{}^{j}r_{\beta\alpha}{}^{h}r_{\alpha 0}{}^{i}}{(\omega_\beta-\omega)(\omega_\alpha-\omega_l)}+\frac{r_{0\beta}{}^{j}r_{\beta\alpha}{}^{i}r_{\alpha 0}{}^{h}}{(\omega_\beta-\omega)(\omega_\alpha+\omega_s)}\right\}.\quad(4.24)$$

The expressions (4.23) and (4.24) are somewhat complicated, and the results (2.42) and (2.43) derived from the classical oscillator model do not reproduce all the complexities of the quantum-mechanical solutions. However, the two-oscillator model successfully predicts the form of dependence of a and b on the laser and scattered frequencies ω_l and ω_s when these lie close to an electronic transition frequency, $(k/m)^{1/2}$ in the classical model, ω_α or ω_β in the quantum-mechanical result.

The summations over α and β in (4.23) and (4.24) run over all electron–hole pair states and would be more properly written as a sum over all pairs of valence and conduction band indices with an integration over all wave vectors in the Brillouin zone. The variations of $a_{hij}{}^{\nu}$ and b_{hij} with ω_l and ω_s would be in general very difficult to compute, requiring as they do a knowledge of all the electronic wavefunctions and eigenvalues together with the deformation-potential matrices. Theories of the resonance behavior of the a and b coefficients and hence of the scattering cross section have so far been applied only to situations where the summations and integrations can be restricted to a small subset of the complete set of electron states.

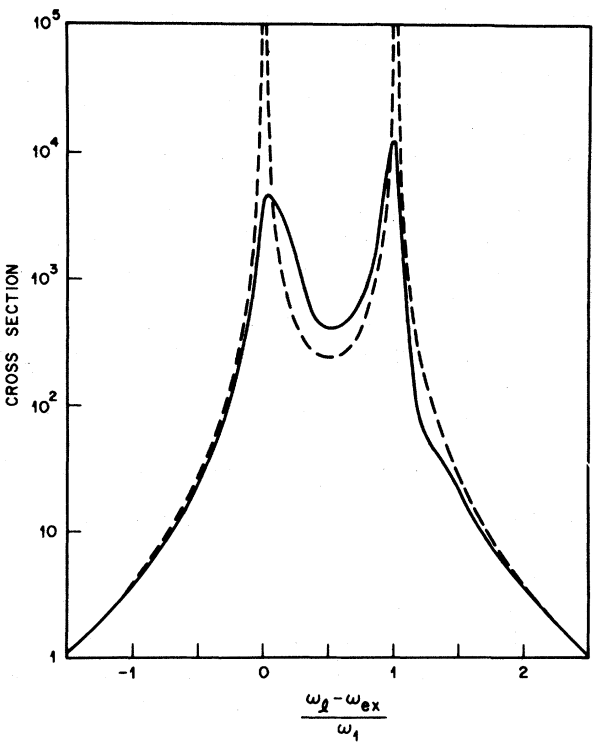

FIG. 17. Scattering cross section in arbitrary units as a function of laser frequency ω_l close to an exciton resonance ω_{ex}. The numerical values assumed for the various parameters are listed in the text. The full curve shows the exact result; the dashed curve is the result obtained by neglecting exciton damping aud taking the refractive indices constant. Note that resonances occur both at $\omega_l=\omega_{ex}$ and at $\omega_s=\omega_l-\omega_l=\omega_{ex}$.

A particularly simple case occurs when the laser frequency lies close to a single exciton peak in the absorption spectrum. Experimentally determined scattering cross sections often show a strong resonant enhancement as the laser frequency approaches the exciton frequency suggesting a theoretical approximation where only the exciton transition is retained in the sums over electronic states. We derive an expression for this case, and then comment on the several publications where results for the same problem have been obtained. It should be realized that the restriction to a single exciton transition will not be a good approximation in all cases, and Bendow *et al.* (1970) have used the entire

range of exciton transitions in comparing theory with experimental results on CdS.

Let us consider the simplest possible case of right-angle scattering by the transverse vibration in a cubic crystal. We assume the incident laser light to be directed along the crystal x axis and polarized parallel to the z axis. The scattered light is observed in the y direction. The standard symmetry rules for light scattering (reviewed by Loudon, 1964) show that $a_{xzy}{}^1$ is the only appropriate nonvanishing coefficient. Thus the scattered light is polarized parallel to x and only the cos $(\pi/4)$ component of the transverse vibrational polarization parallel to y contributes. Thus from (3.61) we have

$$a_T = 2^{-1/2} a_{xzy}{}^1 \tag{4.25}$$

and the integrated cross section obtained from (3.71) is

$$d\sigma/d\Omega = \{\hbar n_s V^2 \omega_s{}^3 \omega_l \mid a_{xzy}{}^1 \mid^2 [n(\omega_1)+1]\}/4\pi n_l c^4 M_1 \omega_1. \tag{4.26}$$

In common with other treatments of resonant light scattering we retain only the most resonant term in the coefficient $a_{xzy}{}^1$. This is the third term in the large bracket of (4.23). It is seen that the frequency dependence of this term near resonance exactly reproduces that of the classical result (2.42). The remaining nonresonant terms could be retained at the expense of making the algebra more tedious, and indeed the work of Ralston *et al.* (1970) shows that the nonresonant terms can sometimes combine with the resonant term to produce interesting cancellations in the cross section. However, we shall here keep only the one term for the sake of simplicity. We denote the exciton frequency by ω_{ex}, the matrix elements of r between the crystal ground state and the exciton state by r_{ex}, and the deformation potential which couples the exciton to the transverse phonon by Ξ_{ex}.

One further modification is necessary before the scattering coefficient can be used to calculate resonant effects. The expressions (2.42) and (4.23) treat the electronic levels as infinitely sharp, whereas experiment and more accurate theories show that damping is present, leading in a first approximation to exciton line shapes which are Lorentzian. Damping effects can be taken care of by writing the exciton frequency as $\omega_{ex} - i\gamma$; then 2γ is the width at half-maximum height of the exciton peak in the absorption spectrum.

With these modifications, the scattering coefficient from (4.23) becomes

$$a_{xzy}{}^1 = \left(\frac{e^2}{\hbar^2 dV}\right)\left(\frac{r_{ex}{}^x \Xi_{ex}{}^y r_{ex}{}^z}{(\omega_{ex}-\omega_s-i\gamma)(\omega_{ex}-\omega_l-i\gamma)}\right), \tag{4.27}$$

and the cross section (4.26) is

$$\frac{d\sigma}{d\Omega} = \frac{n_s \omega_s{}^3 \omega_l e^4 [r_{ex}{}^x \Xi_{ex}{}^y r_{ex}{}^z]^2 [n(\omega_1)+1]}{4\hbar^3 n_l c^4 M_1 \omega_1 d^2 [(\omega_{ex}-\omega_s)^2+\gamma^2][(\omega_{ex}-\omega_l)^2+\gamma^2]}. \tag{4.28}$$

The main frequency dependence of this expression in the resonance region arises from the two Lorentzian terms in the denominator, and from the refractive indices n_s and n_l which exhibit the dispersive behavior typical in the region of an absorption line. It should be emphasized that the energy flows (2.54) and (2.55) which arise in the derivation of the scattering cross section involve only the real refractive indices n_s and n_l, and the imaginary parts do not appear in the cross section even though ω_s and ω_l lie in an absorptive region for resonance scattering.

Figure 17 illustrates how the scattering cross section (4.28) varies with ω_l close to resonance. The dashed curve shows the corresponding result in the absence of any exciton linewidth γ, and with the refractive index variation omitted. For the full curve, the refractive index is calculated using the dielectric constant given by (3.6) modified to refer to the exciton resonance and assuming $\epsilon_\infty = 1$ and an exciton strength S_{ex} of magnitude 10^{-2}. The other exciton parameters were taken as $\omega_{ex} = 2\times 10^4$ cm^{-1}, and $\gamma = 20$ cm^{-1}. The transverse phonon frequency is 400 cm^{-1}. These values are typical for a semiconductor, for example, CdS.

A double-peaked structure of the resonant cross section has been predicted by previous authors but has not to our knowledge been observed experimentally in the first-order Raman cross section, although there is evidence in its favor from the results of higher-order Raman experiments (Leite, Scott, and Damen, 1969). Detailed measurements are made difficult by the availability of only a limited number of laser frequencies which may give a coarse-gained scan of the resonance region. In addition, the theoretical cross section (4.28) relates the incident and scattered light intensities *inside* the scattering medium, whereas experiments measure cross sections relative to light beams *outside* the medium. The relation between the two types of cross section requires matching of electromagnetic waves at the boundaries of the medium and depends upon the geometrical details of a particular

experiment. The boundary conditions can be quite complicated in the resonance region where the light beams are absorbed by the medium, and extraction of a cross section from experimental data to compare with (4.28) is a nontrivial problem in itself.

A range of previous workers have derived expressions for the resonance cross-section at an exciton line. Diverse results have been presented for this same cross section, and it seems worthwhile to discuss the various discrepancies and reconcile the various results with (4.28).

The first treatment of the problem was that of Ovander (1962). No explicit expression for the scattering cross section is given, but the frequency dependence of scattered intensity as ω_l approaches ω_{ex} is discussed under the condition that ω_s remains in a transparent frequency region. A graph is presented showing a three-peaked structure in the scattering cross section as ω_l passes through the resonance region. The theory makes use of the exciton–polariton formed by the interaction of the exciton with the laser photons. We believe that the structure found by Ovander is an artifact of his having used the group velocity of the incident light rather than the energy velocity more appropriate to an absorbing crystal (Loudon, 1970). If a suitable correction is made, the three-peaked structure disappears and the frequency dependence agrees with (4.28).

Birman and Ganguly (1966) and Ganguly and Birman (1967) have presented a theory of light scattering by insulators which includes a consideration of resonant cross sections due to excitons. They omit the exciton damping and the refractive index factors, but their frequency dependence agrees with (4.28) if the same omissions are made. Hopfield (1969) has derived a resonant scattering cross section using the exciton–polariton concept. His result is equivalent to (4.28) with the refractive indices included but without the exciton damping.

Burstein *et al.* (1969) have also treated resonant scattering using the exciton polariton. They state that their result for the frequency dependence of the resonant cross section is qualitatively different from that of Birman and Ganguly mentioned above. However, if Eq. (9) of Burstein *et al.* (1969) is rewritten in terms of the basic exciton parameters instead of various intermediate functions defined in their paper, their result is the same as (4.28) with the following two exceptions: (1) It is necessary to modify (4.28) by retaining the third and fourth terms in (4.23); the fourth term is nonresonant and its retention has little influence on the cross section. (2) Burstein *et al.* neglect the exciton damping γ. Also, as pointed out in their erratum, a factor n_s^2 is omitted in passing from Eq. (8) to (9).

A more complete version of these calculations is given in a more recent paper by Mills and Burstein (1969). We can make contact with the results of this paper as follows. For zero damping the refractive index n is given by

$$n^2=\epsilon=\epsilon_\infty+[S_{ex}\omega_{ex}^2/(\omega_{ex}^2-\omega^2)]. \quad (4.29)$$

Thus very close to resonance we have

$$n\propto(\omega_{ex}-\omega)^{-1/2} \quad (4.30)$$

and if ω_l and ω_s are both close to resonance and for zero damping, (4.28) gives

$$d\sigma/d\Omega\propto[(\omega_{ex}-\omega_s)^{5/2}(\omega_{ex}-\omega_l)^{3/2}]^{-1}. \quad (4.31)$$

The result of Mills and Burstein differs from this by a factor $(\omega_{ex}-\omega_s)$ due to the n_s^2 discrepancy. If only ω_l is close to resonance, n_s can be taken constant, and our result for the main frequency dependence agrees with Mills and Burstein, except that the relevant equation (the second equation on page 1487 of this reference) has a misprint in that the last exponent should be -2 instead of -1.

The most recent theoretical paper on resonance scattering is that of Bendow and Birman (1970). They use exciton polaritons and derive results which are similar to those of other calculations of this kind described above. They present graphs of cross-sections as functions of ω_l and find the characteristic double-peaked structure of Fig. 17.

The main conclusion therefore is that the rather extensive literature on the theory of light scattering at an exciton resonance in the main agrees with the theory given here, leading to (4.28). Where discrepancies occur they seem to be resolvable in terms of factors which have been overlooked by the authors concerned.

F. Stimulated Raman Effect

The stimulated Raman effect lies within the scope of nonlinear optics, and is not of great relevance for the present review. However, the nonlinear parameters which control the gain in a stimulated experiment are simply related to the scattering cross sections given above for spontaneous light scattering, and it is interesting to make the connection with nonlinear optics. A full treatment of the stimulated Raman effect can be found in a review by Bloembergen (1967).

In a stimulated light-scattering experiment, one sets up a scattered light beam whose intensity grows exponentially with its path distance x in the crystal,

$$|E_s(x)|^2=|E_s(0)|^2\exp gx. \quad (4.32)$$

Several authors (e.g., Hellwarth, 1963; Bloembergen, 1967) have derived a relation between the gain g and the spontaneous cross section. In the notation of the present article we have

$$g=(d^2\sigma/d\Omega d\omega_s)\times\{4\pi^2c^3n_l|E_l|^2/V[n(\omega)+1]\hbar\omega_l\omega_s^2n_s^2\}. \quad (4.33)$$

Expressions are often derived for the maximum gain which occurs at the peak of the scattering cross section. As an illustration, we take the cross section (3.69) for a cubic crystal having a single vibrational mode. The maximum gain occurring at $\omega=\omega_0$ is found by inserting (3.69) into (4.33),

$$g_{\max}=(4\pi V\omega_s \mid E_l \mid^2/cM_1\Gamma_1\omega_0 n_s) \times \mid a_T+b_T(M_1/Z_1)(\omega_1^2-\omega_0^2) \mid^2, \quad (4.34)$$

where (3.67) has been used. This expression does not apply when ω lies between the transverse and longitudinal frequencies ω_1 and ω_L. In this frequency region, known as the stop band, it is not possible to set $\omega=\omega_0$ in (3.69) because the undamped polariton dispersion relation (3.65) has no solutions. The maximum gain thus falls off with a Lorentzian tail as the frequency ω is moved into the stop band from either above or below.

For the low-power lasers usually employed in spontaneous Raman scattering experiments, the growth of the scattered wave is comparatively insignificant. However, using high-power pulsed lasers, $g_{\max}$ may attain values as large as 10 cm^{-1} in certain materials.

The polariton produced in a stimulated scattering experiment is a mixture of vibrational and electromagnetic excitation. In nonlinear optics, scattering which generates a vibrational excitation is usually called the stimulated Raman effect, while the generation of a purely electromagnetic excitation is called parametric amplification. Generation of polaritons is clearly a mixture of the two processes, and treatments based on the usual theory of nonlinear optics must embrace both stimulated Raman effect and parametric amplification. The original treatments were given by Butcher *et al.* (1965), Shen (1965), and Henry and Garrett (1968). This last reference obtains an expression for $g_{\max}$ which is identical to (4.34). A figure of the maximum gain as a function of polariton frequency for GaP has been given by Loudon (1969) (see Fig. 7 of this reference) using the theory described here. This figure is the same as would be obtained by plotting the peak height in Fig. 4(a) as a function of frequency. Scott and Ushioda (1969) have given calculated curves of integrated polariton scattering cross section in α quartz, as mentioned in Sec. 4.F. These curves also give an indication of the gain as a function of frequency in a stimulated Raman experiment. It should be noted that for α quartz the cross section can have spikes where the polariton frequency is equal to a pure vibrational frequency, in contrast with GaP where the cross section is a smooth curve having no increase at the transverse lattice vibration frequency. The relative simplicity of the GaP curve results from the way in which the theoretical expressions simplify for a cubic crystal having a single vibrational mode, as mentioned at the end of Sec. 3.

Experiments on stimulated Raman scattering by polaritons have been carried out by Kurtz and Giordmaine (1969), Gelbwachs *et al.* (1969), and Yarborough *et al.* (1969) on $LiNbO_3$. The polaritons produced in such experiments can partially escape from the crystal as infrared radiation, leading to the possibility of a tunable infrared source (Johnson *et al.*, 1971).

ACKNOWLEDGMENTS

We have greatly benefitted from discussions with G. D. Boyd, B. I. Halperin, and D. E. McCumber.

REFERENCES

Abrikosov, A. A., L. P. Gorkov, and I. E. Dzyaloshinski, 1963, *Methods of Quantum Field Theory in Statistical Physics* (Prentice Hall, Englewood Cliffs) p. 258.
Barker, Jr., A. S., 1964, Phys. Rev. **136,** A1290.
——, 1968, Phys. Rev. **165,** 917.
——, 1970, *Far Infrared Properties of Solids*; edited by S. S. Mitra and S. Nudelman (Plenum Press, N.Y., 1970).
——, and R. Loudon, 1967, Phys. Rev. **158,** 433.
Bendow, B., and J. L. Birman, 1970, Phys. Rev. **B1,** 1678.
——, J. L. Birman, A. K. Ganguly, T. C. Damen, R. C. C. Leite, and J. F. Scott, 1970, Optics Commun. **1,** 267.
Benson, H. J., and D. L. Mills, 1970a, Phys. Rev. **B1,** 4835.
——, and D. L. Mills, 1970b, Solid State Commun. **8,** 1387.
Birman, J. L., and A. K. Ganguly, 1966, Phys. Rev. Letters **17,** 647.
Bloembergen, N., 1967, Am. J. Phys. **35,** 989.
Born, M., and K. Huang, 1954, *Dynamical Theory of Crystal* Lattices (Clarendon Press, Oxford).
Boyd, G. D., and D. A. Kleinman, 1968, Phys. Rev. **39,** 3597.
Burstein, E., 1969, Comments Solid State Phys. **1,** 202.
——, and D. L. Mills, 1969a, Comments Solid State Phys. **2,** 93.
——, and D. L. Mills, 1969b, Comments Solid State Phys. **2,** 111.
——, D. L. Mills, A. Pinczuk and S. Ushioda, 1969, Phys. Rev. Letters **22,** 348, Erratum, *ibid.*, **22,** 913.
Butcher, P. N., R. Loudon, and T. P. McLean, 1965, Proc. Phys. Soc. **85,** 565.
——, and N. R. Ogg, 1965, Proc. Phys. Soc. **86,** 699.
Case, K. M., and S. C. Chiu, 1970, Phys. Rev. **A1,** 1170.
Coffinet, J. P., and F. De Martini, 1969, Phys. Rev. Letters **22,** 60.
Couture, L., M. Krauzman, and J. P. Mathieu, 1970, C. R. Acad. Sci. **270,** 1246.
DiDomenico, Jr., M., S. H. Wemple, S. P. S. Porto, and R. P. Bauman, 1968, Phys. Rev. **174,** 522.
Faust, W. L., and C. H. Henry, 1966, Phys. Rev. Letters **17,** 1265.
——, C. H. Henry, and R. H. Eick, 1968, Phys. Rev. **173,** 781.
Ganguly, A. K., and J. L. Birman, 1967, Phys. Rev. **162,** 806.
Garrett, C. G. B., 1968, IEEE Transactions on Quantum Electronics **QE-4,** 70.
Gelbwachs, J., R. H. Pantell, H. E. Puthoff, and J. M. Yarborough, 1969, Appl. Phys. Letters **14,** 258.
Hartwig, C. M., E. Wiener-Avnear, J. Smit, and S. P. S. Porto, 1971, Phys. Rev. **B3,** 2078.
Hellwarth, R. W., 1963, Phys. Rev. **130,** 1850.
Henry, C. H., and C. G. B. Garrett, 1968, Phys. Rev. **171,** 1058.
——, and J. J. Hopfield, 1965, Phys. Rev. Letters **15,** 964.
Hopfield, J. J., 1966, *Proceedings of the International Conference on the Physics of Semiconductors*, (J. Phys. Soc. Japan Suppl. **21**).
——, 1969, Phys. Rev. **182,** 945.
Huang, K., 1951, Proc. Roy. Soc. **A208,** 352.
Johnson, B. C., H. E. Puthoff, J. Soohoo, and S. S. Sussman, 1971, Appl. Phys. Letters **18,** 181.
Johnston, Jr., W. D., 1970, Phys. Rev. **B1,** 3494.
——, and I. P. Kaminow, 1969, Phys. Rev. **188,** 1209.
Kaminow, I. P., 1967, *Ferroelectricity*, edited by E. F. Weller, (Elsevier, New York) p. 183.

——, 1969, *Light Scattering Spectra of Solids*, edited by G. B. Wright, (Springer-Verlag, New York) p. 678.
——, and T. C. Damen, 1968, Phys. Rev. Letters **20,** 1105.
——, and W. D. Johnston, Jr., 1967, Phys. Rev. **160,** 519, also 1969 Phys. Rev. **178,** 1528.
Kittel, C., 1958, *Elementary Statistical Physics*, (Wiley, New York) Part 2, and Sec. 44.
——, 1969, *Thermal Physics* (Wiley, New York).
Klyshko, D. N., A. N. Penin, and B. F. Polkovnikov, 1970, JETP Letters **11,** 5.
Koster, G. F., J. O. Dimmock, R. G. Wheeler, and H. Statz, 1963, *Properties of the Thirty-two Point Groups* (M.I.T. Press, Cambridge, Mass.).
Krauzman, M., 1970, C. R. Acad. Sci. **B270,** 856.
Kurtz, S. K., and J. A. Giordmaine, 1969, Phys. Rev. Letters **22,** 192.
Landau, L. D., and E. M. Lifshitz, 1969, *Statistical Physics*, (Pergamon Press Ltd., London), 2nd edition, Chap. 12.
Lax, M., 1960, Rev. Mod. Phys. **32,** 25.
Leite, R. C. C., T. C. Damen, and J. F. Scott, 1969, *Light Scattering Spectra of Solids* (Springer-Verlag, New York) p. 359.
——, J. F. Scott, and T. C. Damen, 1969, Phys. Rev. Letters **22,** 780.
Loudon, R., 1963a, Proc. Phys. Soc. **82,** 393.
——, 1963b, Proc. Roy. Soc. **A275,** 218.
——, 1964, Adv. Phys. **13,** 423; Adv. Phys. **14,** 621, 1965.
——, 1969, *Light Scattering Spectra of Solids*, edited by G. B. Wright (Springer-Verlag, New York) p. 25.
——, 1970, J. Phys. **A3,** 233.
MacDonald, D. K. C., 1962, *Noise and Fluctuations* (Wiley, New York).
Mills, D. L., and E. Burstein, 1969, Phys. Rev. **188,** 1465.
Obukhovskii, V. V., H. Ponath, and V. L. Strizhevskii, 1970, Phys. Stat. Sol. **41,** 837; also **41,** 847.
Ovander, L. N., 1962, Sov. Phys. Solid State **4,** 1081.
Peierls, R. E., 1955, *Quantum Theory of Solids*, (Clarendon Press, Oxford).
Pinczuk, A., E. Burstein, and S. Ushioda, 1969, Solid State Communications **7,** 139.
Porto, S. P. S., B. Tell, and T. C. Damen, 1966, Phys. Rev. Letters **16,** 450.
Poulet, H., 1955, Ann. Phys. Paris **10,** 908.
Puthoff, H. E., R. H. Pantell, B. G. Huth, and M. A. Chacon, 1968, J. Appl. Phys. **39,** 2144.
Ralston, J. M., R. L. Wadsack, and R. K. Chang, 1970, Phys. Rev. Letters **25,** 814.
Scott, J. F., L. E. Cheesman, and S. P. S. Porto, 1967, Phys. Rev. **162,** 834.
——, T. C. Damen, J. Ruvalds, and A. Zawadowski, 1971, Phys. Rev. **B3,** 1295.
——, and S. Ushioda, 1969, *Light Scattering Spectra of Solids*, (Springer-Verlag, New York) p. 57.
Shen, Y. R., 1965, Phys. Rev. **138,** A1741.
Stolen, R. H., 1970, Physics Chem. Glasses **11,** 83.
Westman, H. P., 1961, *Reference Data for Radio Engineers* edited by H. P. Westman (American Book-Stratford Press, New York) Chap. 5.
Yarborough, J. M., S. S. Sussman, H. E. Puthoff, R. H. Pantell, and B. C. Johnson, 1969, Appl. Phys. Letters **15,** 102.
Zallen, R., G. Lucovsky, W. Taylor, A. Pinczuk, and E. Burstein, 1970, Phys. Rev. **B1,** 4058.